Available online at www.sciencedirect.com
SCIENCE DIRECT®
Geochimica et Cosmochimica Acta 70 (2006) 224–245
Geochimica
www.elsevier.com/locate/gca

Li and B isotopic variations in an Allende CAI: Evidence for the in situ decay of short-lived ^{10}Be and for the possible presence of the short-lived nuclide ^{7}Be in the early solar system

Marc Chaussidon [a,*], François Robert [b], Kevin D. McKeegan [c]

[a] *CRPG-CNRS, BP 20, 54501 Vandoeuvre-lès-Nancy, France*
[b] *LEME-MNHN-CNRS, 61 rue Buffon, 75005 Paris, France*
[c] *Department of Earth and Space Sciences, UCLA, Los Angeles, CA 90095-1567, USA*

Received 6 October 2004; accepted in revised form 18 August 2005

Abstract

The concentrations and isotopic compositions of lithium, beryllium, and boron, analyzed in situ by ion microprobe in 66 spots of a type B1 Ca–Al-rich inclusion (CAI 3529-41) from the Allende meteorite, are reported. Large variations are observed for both the Li and the B isotopic ratios with ^{7}Li/^{6}Li ranging from 9.2 ± 0.22 to 12.22 ± 0.43 (a ≈250‰ range in δ^{7}Li values) and ^{10}B/^{11}B ranging from 0.2468 ± 0.0057 to 0.4189 ± 0.0493 (a 410‰ range in δ^{11}B values). The very low Li concentrations (<1 ppb) observed in several anorthite and fassaite grains require that a correction for the contribution of spallogenic Li produced during irradiation of the Allende meteoroid by galactic cosmic rays (GCR) be made (after this correction ^{7}Li/^{6}Li ranges from 9.2 ± 0.22 to 13.44 ± 0.56, i.e., a ≈350‰ range in δ^{7}Li values). In 3529-41, the ^{10}B/^{11}B ratios are positively correlated with ^{9}Be/^{11}B in a manner indicating the in situ decay of short-lived ^{10}Be (half-life = 1.5 Ma) with a ^{10}Be/^{9}Be ratio at the time of formation of the CAI of $8.8 \pm 0.6 \times 10^{-4}$, which is in agreement with previous findings [McKeegan, K.D., Chaussidon, M., Robert, F., 2000. Incorporation of short-lived ^{10}Be in a calcium–aluminum-rich inclusion from the Allende meteorite. *Science* **289**, 1334–1337]. The present detailed investigation demonstrates that only minor perturbations of the ^{10}Be–^{10}B system are present in 3529-41, contrary to the ^{26}Al/^{26}Mg system for which numerous examples of isotopic redistribution following crystallization were observed [Podosek, F.A., Zinner, E.K., MacPherson, G.J., Lundberg, L.L., Brannon, J.C., Fahey, A.J., 1991. Correlated study of initial ^{87}Sr/^{86}Sr and Al–Mg systematics and petrologic properties in a suite of refractory inclusions from the Allende meteorite. *Geochim. Cosmochim. Acta* **55**, 1083–1110]. Petrographically based criteria were developed to identify within the 66 analyzed spots in 3529-41, those where post-magmatic perturbation of the Li and Be distributions occurred. Li and Be concentrations measured in different analytical spots are compared with those predicted by using experimentally determined partition coefficients according to a model of closed-system crystallization of the CAI melt. These criteria show that 56% of the spots in melilite, 38% in anorthite, and 8% in fassaite suffered post-crystallization perturbations of Li and/or Be distributions. In the remaining spots, which do not show obvious indication of redistribution of Li or Be, the ^{7}Li/^{6}Li isotopic variations (corrected for GCR exposure) are positively correlated with ^{9}Be/^{6}Li suggesting the in situ decay of now-extinct ^{7}Be. The derived isochron implies that at the time of its formation, the CAI melt had a ^{7}Be/^{9}Be ratio of 0.0061 ± 0.0013 and a ^{7}Li/^{6}Li ratio of 11.49 ± 0.13. In contrast, all the spots in 3529-41, which do show evidence for post-magmatic redistribution of Li and Be, have relatively constant ^{7}Li/^{6}Li, averaging 11.72 ± 0.56, which is consistent with mass balance calculations for Li isotopic homogenization in the CAI after the decay of ^{7}Be. The incorporation of live ^{7}Be in 3529-41 requires, because of the very short half-life of this nuclide (53 days), that it be produced essentially contemporaneously with the formation of the CAI. Therefore, the irradiation processes responsible for production of ^{7}Be must have occurred within the solar accretion disk. Calculations developed in the framework of the x-wind model [Gounelle, M., Shu, F.H., Shang, H., Glassgold, A.E., Rehm, E.K., Lee, T., 2004. The origin of short-lived radionuclides and early Solar System irradiation (abstract). *Lunar Planet. Sci.* **35**, 1829] reproduce the ^{7}Be and ^{10}Be abundances observed in 3529-41. The correlated presence of ^{7}Be and ^{10}Be in 3529-41 is thus a strong

* Corresponding author. Fax: +33 83 51 17 98.
E-mail addresses: chocho@crpg.cnrs-nancy.fr (M. Chaussidon), robert@mnhn.fr (F. Robert), mckeegan@ess.ucla.edu (K.D. McKeegan).

0016-7037/$ - see front matter © 2005 Elsevier Inc. All rights reserved.
doi:10.1016/j.gca.2005.08.016

argument that ^{10}Be, which is observed rather ubiquitously in CAIs, is also a product of irradiation in the early solar system, as might be a significant fraction of other short-lived radionuclides observed in early solar system materials.
© 2005 Elsevier Inc. All rights reserved.

1. Introduction

The discovery in Ca-, Al-rich inclusions (CAIs) from carbonaceous chondrites of isotopic anomalies in boron due to the in situ decay of short-lived ($T_{1/2} = 1.5$ Ma) ^{10}Be (MacPherson et al., 2003; McKeegan et al., 2000; Sugiura et al., 2001) has renewed an old idea according to which a fraction of primitive solar system materials underwent irradiation by energetic particles from the young Sun. Independently, X-ray observations of low-mass stars in pre-T-Tauri and T-Tauri phases have suggested that these young stellar objects are a source of an intense flux of accelerated particles (Feigelson and Montmerle, 1999). Recent X-ray observations in the Orion nebular cluster of 43 young stellar objects with ages from <0.3 to ≈10 Ma and masses ranging from 0.7 to 1.4 $M_{\odot}$ demonstrate that essentially all solar-type stars go through an epoch of greatly enhanced X-ray luminosity (Feigelson et al., 2002). Scaling of X-ray luminosity leads to estimates of enhancement factors of $\sim 10^5$ for the proton flux relative to that of the present day Sun, and the population distribution suggests that this high activity lasts for periods of up to a few million years (Feigelson et al., 2002). From the astronomical observations, it seems inevitable that the Sun would have passed through such a phase during its formation and early evolution. Whether or not the components of primitive meteorites witnessed this epoch is a question that, in principle, can be addressed by examining the isotopic records of the earliest solar system rocks.

Models developed to describe the magnetic interaction between a forming star and its accretion disk (Shu et al., 1994) predict the existence close to the star of a gas-free region in which dust grains might be irradiated by energetic particles associated with magnetic reconnection events. Because of its proximity to the accreting star (as close as ~0.06 AU), the dust is severely thermally processed, undergoing a series of evaporation/recondensation events and possibly melting. Surviving distillates or recondensed solids can migrate back to the so-called X region (at the termination of the accretion disk) through fluctuations in the accretion rate and/or magnetic field strength of the accreting star (Gounelle et al., 2001; Lee et al., 1998; Shu et al., 1996, 1997). These irradiated and thermally processed solids can then be launched by a magnetocentrifugal "x-wind" and fall back on the mid plane of the accretion disk at distances of several AU where these refractory solids may agglomerate with thermally unprocessed materials into the parent bodies of primitive meteorites. The presence in CAIs of specific isotopic anomalies due to the irradiation process would be a strong argument in favor of a scenario of the x-wind type for the evolution of early solar system (Lee et al., 1998).

In principle, the isotopic compositions of Li, Be, and B in CAIs can provide significant constraints on the existence of such irradiation processes in the early solar system. Because these elements are destroyed in stellar interiors and are produced primarily by spallation reactions on carbon and oxygen target nuclei, they have relatively low abundances in the solar system (Anders and Grevesse, 1989). Furthermore, the isotopic compositions produced by spallation reactions are energy dependent. For example, the ^{7}Li/^{6}Li ratio produced by high energy (GeV range) galactic cosmic ray (GCR) spallation of O and C nuclei is ≈2 (Meneguzzi et al., 1971), which is much less than the average chondritic ratio of 12.02 (James and Palmer, 2000; McDonough et al., 2003). Calculations indicate that for a range of realistic compositions and energetic spectra the spallation-produced ^{7}Li/^{6}Li ratios are always much lower than 12 (Ramaty et al., 1996), which means that the chondritic ratio must be due to mixing between ^{7}Li produced during the Big-Bang, and ^{7}Li-poor Li produced by spallation reactions at various energies during the evolution of the galaxy (Reeves, 1994). The situation is less clear for B because it is produced during low-energy (MeV range) spallation reactions with various ^{11}B/^{10}B ratios ranging from ~2.5 to 7 (Cassé et al., 1995; Ramaty et al., 1996) which bracket the chondritic value of ^{11}B/^{10}B ≈ 4.04 (Zhai et al., 1996). In general, the low abundances and the strong isotopic contrasts of various spallation sources of Li and B make the isotopic composition of these elements very sensitive to small additions of a specific irradiation-produced component. Finally, two short-lived radioactive isotopes of Be exist: ^{10}Be β-decays to ^{10}B with a half-life of 1.5 My and ^{7}Be decays to ^{7}Li by electron capture with a half-life of 53 days.

The rather systematic incorporation by CAIs of ^{10}Be during their formation (MacPherson et al., 2003; McKeegan et al., 2000; Sugiura et al., 2001) was originally taken as a decisive argument for the presence of irradiation processes in the early solar system (McKeegan et al., 2000). This view was recently challenged (Desch et al., 2004) based on calculations of the concentrations of ^{10}Be that might be achieved by magnetic trapping of GCRs in the molecular cloud parental to the solar system. Although the calculations do not prove that the ^{10}Be observed in CAIs could not have been produced by irradiation around the early Sun, they nevertheless raise the possibility that a significant fraction of it is of pre-solar origin, which is conceivable because of the relatively long half-life of ^{10}Be. Obviously, a definitive argument in favor of a production of Be by solar system irradiation processes would be the incorporation in CAIs of ^{7}Be since its very short half-life precludes any pre-solar heritage. Previous searches for ^{7}Be in CAIs (Chaussi-

don et al., 2001, 2002) have shown that large $^{7}Li/^{6}Li$ isotopic variations are present but no unambiguous "isochron-type" relationship could be demonstrated between the $^{7}Li/^{6}Li$ and the $^{9}Be/^{6}Li$ ratios. The Li isotopic variations in one Allende CAI (USNM 3515) were tentatively explained by a diffusive relaxation during cooling of Li isotopic anomalies due to the in situ decay of ^{7}Be, but no petrographic evidence could be found to support (or deny) this interpretation (Paque et al., 2003). Another problem with the study of USNM 3515 was that this inclusion showed anomalously high B concentrations (in the ppm range) precluding the detection of ^{10}Be in it.

In the present study, we report detailed analyses of the Li–Be–B isotopic compositions of another Allende CAI (3529-41), which is known to have contained ^{10}Be (McKeegan et al., 2000) at close to the highest level found so far in any CAI. The petrology of 3529-41 was previously studied by Podosek et al. (1991) who also demonstrated that it contained ^{26}Al at close to the canonical value at the time of its formation (Podosek et al., 1991). Our data show that correlations exist between CAI mineralogy and Li–Be concentrations and isotopic compositions suggesting that, when it last crystallized, CAI 3529-41 incorporated live ^{7}Be into its mineral structures.

2. Sample and analytical techniques

2.1. Allende CAI 3529-41

Allende 3529-41 was previously studied for its petrology (major and trace elements) as well as for its Mg and Sr isotopic compositions by Podosek et al. (1991). It is a coarse-grained type B1 CAI according to the definitions of MacPherson et al. (1988) and of Wark and Lovering (1982) containing a melilite-rich mantle surrounding a fassaite + spinel-rich core. In the studied section, the CAI appears irregular in shape with a maximum size of ≈6 mm (Fig. 1). The inclusion is surrounded by a continuous Wark–Lovering rim of ≈70 μm thickness composed from the exterior to the interior of olivine, fassaïte, spinel + perovskite, and secondary anorthite mixed with melilite alteration products. The mantle has an average thickness of ~500 μm and is primarily composed of large melilite crystals, which, however, are not laths radiating inwards. Accessory spinel, fassaïte, and anorthite appear concentrated in a few zones within the melilite mantle. The core of the inclusion is made of melilite (with the highest Mg contents, from $Åk_{65}$ to $Åk_{74}$, see Table 1A), fassaïte, and anorthite crystals with included euhedral spinel crystals. The melilite in the core appears largely euhedral. The chemical compositions of the different phases

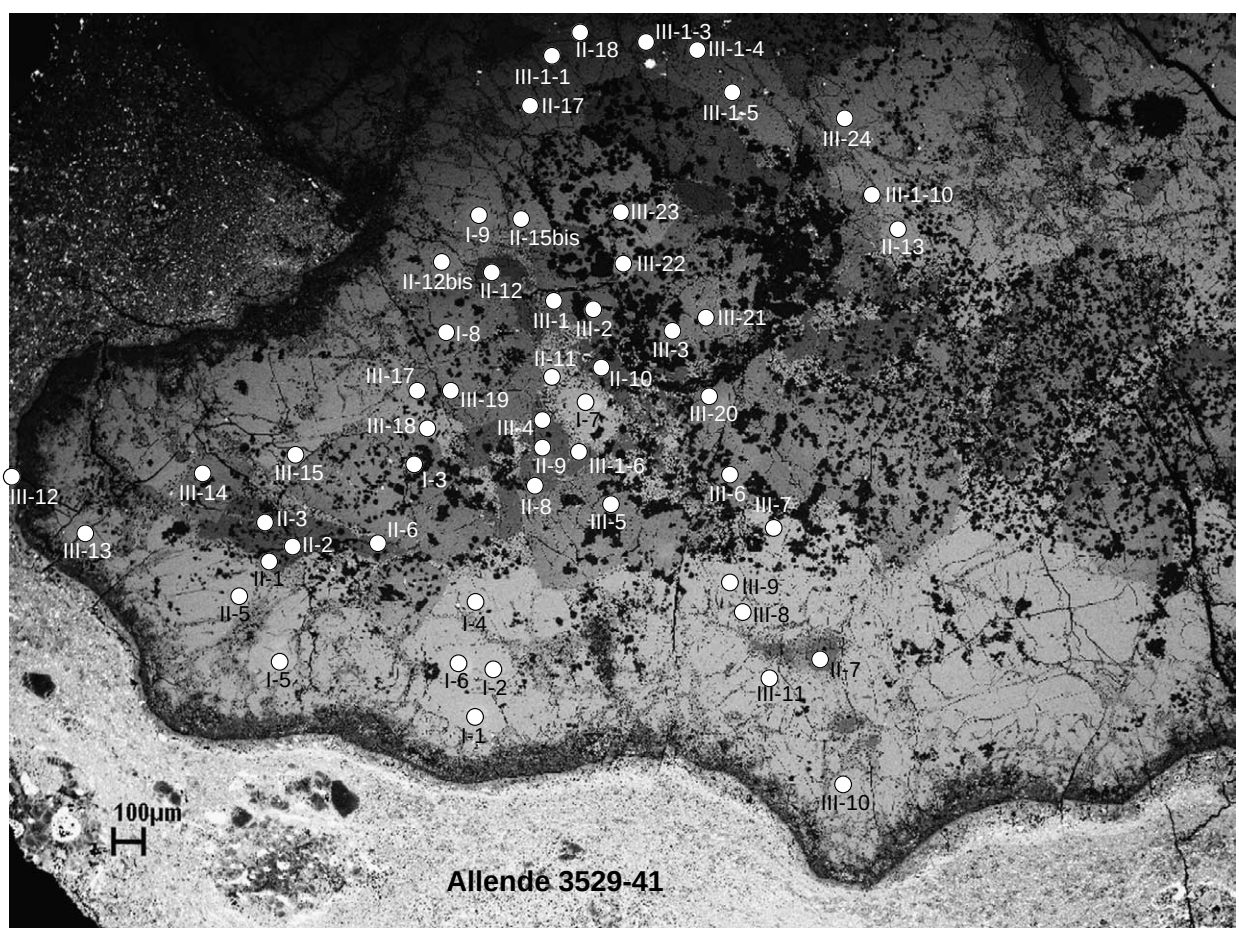

Fig. 1. Backscattered electron image of CAI 3529-41 with location of analytical spots.

Table 1A
Major element compositions of melilite in 3529-41

Spot #	SiO_2	TiO_2	Al_2O_3	Cr_2O_3	FeO	MnO	MgO	CaO	Na_2O	Total
I.1	28.29	0.03	27.51	—	0.03	0.05	4.06	41.71	0.03	101.73
I.2	30.63	0.23	23.68	—	0.03	—	5.47	41.05	—	101.12
I.4	30.84	0.03	22.93	—	—	—	5.79	41.16	0.11	100.93
I.5	29.49	0.05	25.94	—	—	—	4.57	41.50	0.08	101.65
I.6	30.76	—	22.78	—	0.04	0.03	5.86	41.64	0.03	101.17
I.9	30.89	0.03	23.28	—	—	—	5.69	41.64	—	101.58
II.5(1)	29.74	—	25.03	—	—	—	5.01	41.35	0.05	101.23
II.13	33.49	—	18.18	—	—	0.04	7.72	41.70	0.21	101.38
II.12bis	29.39	—	25.30	—	—	—	4.87	41.97	0.15	101.69
II.15bis	32.87	—	20.21	—	—	—	6.82	41.44	0.23	101.57
II.17	29.25	—	24.77	—	—	—	5.17	41.40	0.12	100.73
II.18	29.42	—	25.36	—	—	—	4.96	41.64	0.08	101.49
III.1-1	30.26	0.48	23.45	—	—	—	5.62	40.73	0.12	100.71
III.1-3	29.26	—	24.77	—	0.06	—	4.97	41.46	0.04	100.61
III.1-4	28.96	—	24.52	—	0.07	—	5.35	41.51	0.04	100.49
III.1-5	29.83	—	24.37	—	0.03	0.03	5.29	41.68	—	101.29
III.1-10	31.83	—	21.05	—	—	0.04	6.52	41.67	0.19	101.34
III.7	33.14	—	19.63	—	—	—	6.90	41.25	0.16	101.09
III.8	29.69	—	25.16	—	0.08	—	4.89	41.51	0.08	101.44
III.9	29.40	—	25.53	—	—	—	4.79	40.98	0.05	100.75
III.10	28.96	—	25.43	—	—	—	4.77	41.82	0.12	101.16
III.11	31.54	0.13	22.51	—	—	—	6.09	41.81	—	102.10
III.13(1)	27.81	—	28.57	—	0.04	0.04	3.45	41.25	0.11	101.31
III.15(1)	32.04	—	20.23	—	0.05	—	6.80	41.42	0.16	100.71
III.18(1)	35.46	—	12.91	—	0.05	—	9.80	41.56	0.24	100.04
III.22	34.27	—	15.75	—	—	0.04	8.57	41.22	0.20	100.10
III.23	30.04	—	24.61	0.03	—	—	5.22	41.24	—	101.18
III.24	28.40	0.10	25.60	—	1.20	—	4.65	40.66	0.05	100.65
IV.1	28.85	—	25.82	—	—	0.03	4.77	41.81	0.05	101.34
IV.2	28.93	0.03	26.56	—	0.04	—	4.45	41.61	—	101.65
IV.3	28.01	—	27.21	—	—	0.03	4.16	41.65	—	101.10

Electron probe analyses performed with a Cameca SX100 instrument at Université Henri Poincaré (Nancy) using standard procedures. Data are, in most cases, the average of two spots made as close as possible of the ion probe spot (the variations between the two spots are in average of 4% relative for major elements with, in some cases, variations of up to 20% relative).
—, Below detection limit (0.03 wt%).

(pyroxene, anorthite, and melilite) analyzed by ion probe for Li and B isotopic compositions are given in Tables 1A and 1B. They do not show any significant peculiarities compared to previous detailed studies of type B CAIs (e.g., Brearley and Jones, 1998; Grossman, 1975; Simon et al., 1991).

Podosek et al. (1991) presented detailed studies of the Na_2O distributions in melilite at the micrometer scale in Allende 3529-41, observing that many melilite crystals showed an irregular variation of Na_2O contents, together with an irregular variation of the Åk content. A clear correlation between Na_2O and Åkermanite contents in melilite is not observed for Åk < 40%, neither within single zoned crystals (Figs. 6 and 7 of Podosek et al., 1991) nor between different crystals at the scale of the whole CAI (Table 1A).

While a clear Al–Mg isochron was observed in anorthite and fassaite, giving an initial $^{26}Al/^{27}Al$ ratio of $4.1 \pm 1.2 \times 10^{-5}$, Podosek et al. (1991) noticed that extensive perturbations of the Al–Mg system were present in melilite. In a few cases, the authors could relate these perturbations to spikes (positive or negative) in the Na concentrations of the melilite.

In conclusion, petrographic data indicate that Allende CAI 3529-41 has many characteristics typical of a type B1 CAI. Subsequent to its original magmatic history, it suffered several perturbations as evidenced by the brecciation of the CAI, the variations of the Na_2O contents in melilite, and the disturbance of the Al–Mg system in melilite. We decided, however, to study this CAI in detail for Li and B isotopic compositions because: (i) a preliminary survey showed it has locally very high Li isotopic ratios compared to those of other CAIs we studied (Chaussidon et al., 2001, 2002), (ii) it is coarse-grained allowing the Li–Be–B analyses with large spot size (see next section), (iii) previous measurements indicated that it formed with live ^{10}Be (McKeegan et al., 2000), and (iv) the perturbations evidenced from Na_2O contents and the Al–Mg systematics were studied in detail (Podosek et al., 1991).

2.2. Ion microprobe analyses

Li–Be–B concentrations and isotopic compositions were measured with the CRPG-CNRS Cameca ims 1270 ion microprobe using the same standards (Table 2) and procedures as the ones developed on the ims 3f (Chaussidon and Robert, 1998; Chaussidon et al., 1997) and previously described for the ims 1270 (McKeegan et al.,

Table 1B
Major element compositions of fassaite, anorthite, and Wark–Lovering rim (bulk) in Allende 3529-41

Spot #	SiO_2	TiO_2	Al_2O_3	Cr_2O_3	FeO	MnO	MgO	CaO	Na_2O	Total
Fassaite										
I.8	35.74	10.65	21.63	0.09	—	—	7.42	25.29	—	100.85
III.1	40.54	5.15	20.21	0.07	—	—	9.49	25.50	—	100.97
III.2	41.82	4.85	18.69	0.08	—	—	10.09	25.56	0.04	101.14
III.3(1)	38.12	7.61	20.74	0.05	—	0.03	8.64	25.76	0.08	101.05
III.6	40.57	5.04	20.60	0.07	—	—	9.43	25.80	—	101.55
III.14	36.50	9.64	21.36	0.08	—	—	7.84	25.38	—	100.84
III.17	37.96	7.58	21.20	0.04	—	—	8.70	25.53	—	101.02
III.19(2)	37.67	7.85	21.14	0.05	0.06	—	8.45	25.39	—	100.66
III.20	39.49	5.79	19.92	0.10	0.05	0.06	9.69	25.56	—	100.67
III.21	38.14	8.96	19.59	0.08	—	—	8.58	25.41	0.04	100.82
Anorthite										
II.1	40.76	0.03	34.58	—	—	—	0.26	23.51	0.14	99.31
II.2	42.89	0.05	37.16	—	0.05	—	0.13	20.64	0.06	101.01
II.3	42.99	0.03	37.92	—	—	0.03	0.08	20.65	0.06	101.81
II.4	43.30	0.05	37.86	—	—	—	0.05	20.63	0.08	102.00
II.7(1)	42.52	0.04	36.91	—	—	—	0.11	20.67	0.10	100.37
II.12	43.44	0.08	38.01	—	—	—	0.19	20.78	0.08	102.60
Wark–Lovering rim										
III.12	48.29	0.67	9.56	0.07	3.19	0.08	14.31	24.04	0.28	100.50

Electron probe analyses performed with a Cameca SX100 instrument at Université Henri Poincaré (Nancy) using standard procedures. Data are, in most cases, the average of two spots made as close as possible of the ion probe spot (the variations between the two spots are in average of 4% relative for major elements with, in some cases, variations of up to 20% relative).
—, Below detection limit (0.03 wt%).

2000). The sample was sputtered with a 12.5 kV O^- primary beam of high intensity (≈50 nA but in some cases up to ~120 nA), this intensity being necessary to obtain sufficient counts on the Li–Be–B peaks for precise isotopic measurements. This beam produced sample craters of ≈50–80 μm diameter and several micrometer depth. Positive secondary Li–Be–B ions were accelerated through 10 kV and analyzed at sufficient mass resolution ($M/\Delta M \approx 2000$) to separate all possible interferences on the Li–Be–B peaks while maintaining essentially full transmission of the spectrometer. All the Li–Be–B isotopes were counted in mono-collection mode on the central electron multiplier. No correction was applied for electron multiplier dead time because the secondary ion intensities were always below 10^4 counts/s. The energy slit was centered and opened to accept an energy band pass of ±45 eV. Charging of the sample was generally small (≈5–10 V measured after 1h30 sputtering).

The sample (a conventional petrographic thin section) was carbon coated and the analytical spots were chosen from the secondary electron microscope map to avoid as much as possible cracks and microphases (Fig. 1). However, because of the large size of the primary beam compared to the size of the minerals in 3529-41, it proved impossible to focus the beam onto only mono-mineralic phases. For this reason, the analytical spots were chosen by checking for homogeneity of the ion images of Li^+, Be^+, and B^+ which ensured that no major crack or alteration phase (visible in the Li and/or B images) was in the analyzed zone.

The removal of surface contamination was monitored by requiring that the $^{11}B^+$ intensity decrease from a few $\times 10^4$ counts/s at the beginning of a measurement down to approximately a few $\times 10^2$ counts/s. After this pre-sputtering, which typically took ~15 min, the field diaphragm was closed to 1500 μm × 1500 μm (corresponding to an area of ≈15 μm × 15 μm on the sample) and the position of the secondary beam in the field diaphragm was adjusted by using the transfer lens deflectors to minimize contamination coming from the edges of the sputtered craters as seen from the $^7Li^+$ and $^{11}B^+$ ion images. In some cases, the field diaphragm had to be closed to 1000 μm × 1000 μm in order to minimize the contribution from some phases showing higher Li and/or B intensities. It must be mentioned that despite these precautions it was quite obvious that some small phases (mostly spinels) or some secondary phases might have contributed significantly to the Li–Be–B signals emitted from the three major minerals analyzed (melilite, fassaite, and anorthite). In addition, while the $^9Be^+$ intensity was rather stable during an analysis, the Li^+ and B^+ intensities frequently showed a continuous decrease. This decrease indicates that the removal of Li and B ions coming from the periphery of the sputtered area was not always 100% efficient. Finally, in some cases, sharp variations in Li–Be–B intensities were observed in the course of the analysis, indicating that one phase was either exhausted or revealed by the beam. In these cases, the analysis was split in two and these points are indicated by a number in brackets in Tables 3A, 3B and 4A, 4B (see Supplementary material figures EA1 and EA2).

Table 2
Li–Be–B useful yields and instrumental mass fractionations during ion microprobe analysis[a]

Standard[b]	$Yield_{Li/Be}$	2σ[c]	$Yield_{B/Be}$	2σ[c]	$\alpha_{inst}Li$	2σ[c]	$\alpha_{inst}B$	2σ[c]
May-01[c]								
GB4pt1	3.04	0.05	0.389	0.004	1.0266	0.0017	0.9664	0.0010
GB4pt2	2.94	0.05	0.399	0.002	1.0309	0.0010	0.9726	0.0006
Average	2.99	0.07	0.394	0.007	1.0288	0.0031	0.9695	0.0044
September-02								
GB4					1.0456	0.0014	0.9745	0.0016
GB4					1.0397	0.0009	0.9708	0.0017
GB4	3.82		0.366		1.0412	0.0010	0.9737	0.0015
GB4	3.06		0.355		1.0396	0.0012	0.9724	0.0025
Average	3.44	0.54	0.360	0.008	1.0415	0.0028	0.9728	0.0016
2-December-02								
GB4	—	—	—	—	—	—	0.9758	0.0033
BHV0	7.19	0.03	0.561	0.011	1.0408	0.0025	—	—
BHV0	6.04	0.03	0.521	0.003	1.0404	0.0014	—	
Average	6.61	0.81	0.541	0.028	1.0406	0.0003	0.9758	0.0033
18-December-02								
GB4	2.93	0.10	0.367	0.340	1.0423	0.0013	0.9753	0.0012
March-03[d]								
GB4	2.67	0.03	0.350	0.001	1.0414	0.0018	0.9687	0.0017
GB4	2.26	0.02	0.365	0.002	1.0457	0.0016	0.9734	0.0017
GB4	2.44	0.02	0.365	0.005	1.0447	0.0031	0.9706	0.0017
BHV0	6.21	0.02	0.475	0.001	1.0437	0.0019		
Average	3.39	1.89	0.389	0.002	1.0439	0.0018	0.9709	0.0024
April-03								
GB4	4.34	0.02	0.375	0.001	1.0422	0.0009	0.9725	0.0012
GB4	6.29	0.04	0.372	0.001	1.0449	0.0007	0.9737	0.0015
Average	5.31	1.38	0.373	0.002	1.0436	0.0019	0.9731	0.0009
September-03								
GB4	1.06		0.347					
GB4	1.07		0.353					
UTR2	1.24		0.287					
UTR2	1.30		0.367					
UTR2	1.31		0.430					
Average	1.19	0.12	0.357	0.051				

[a] See text for definitions of useful yield and instrumental mass fractionation.
[b] Three glass standards were used, see text for compositions. The dates for each analytical session are indicated. The ion probe settings were different in session September-03 (see text).
[c] Two sigma standard errors of mean.
[d] The two sessions indicated in bold are those corresponding to the new Li–Be–B analyses of CAI 3529-41 presented in this manuscript.

Each analysis consisted of ~15 min pre-sputtering and up to 1h 30 min counting by cycling through masses 5.8 (2 s), ^{6}Li (8 s), ^{7}Li (4 s), ^{9}Be (4 s), ^{10}B (10 s), and ^{11}B (5 s). Analyses in Li- and B-rich areas were shorter and they were stopped when a counting statistic of a few permil uncertainty was reached on the Li and B isotopic ratios. The Li–Be–B ion yields and Li and B instrumental mass fractionations were determined by analyses of a set of three glass standards used in all our previous Li and B analyses: GB4 glass contains 384 ppm Li with $\delta^{7}Li = -4.3 \pm 0.5‰$, 11.3 ppm Be, and 970 ppm B with $\delta^{11}B = -12.8 \pm 0.5‰$; BHV0-1 glass contains 4.6 ppm Li with $\delta^{7}Li = +5.8 \pm 0.5‰$, 1.1 ppm Be, and 2.5 ppm B; UTR 2 contains 63.4 ppm Li, 9 ppm Be, and 17.7 ppm B (analyses by M. Chaussidon at CRPG, J. Stix personal communication, and Govindaraju, 1989). Data for these standards during the two analytical sessions in which 3529-41 was analyzed are given in Table 2 together with analyses of these standards during other Li–Be–B sessions between September 2002 and September 2003.

The $^{9}Be/^{6}Li$ and $^{9}Be/^{11}B$ concentration ratios, which are important in order to look for in situ decay of ^{7}Be and ^{10}Be, were determined after calibration of the ion yields of Li and B relative to Be on the glass standards. While the B^{+}/Be^{+} yields were relatively stable over the different analytical sessions in 2001–2003, the Li^{+}/Be^{+} yields varied significantly (Table 2). These variations are most likely due to differences in the adjustment of the secondary high voltage of the ion probe since Li^{+} and Be^{+} secondary ions have different energy distributions which result in a strong variation of their relative yields with energy (Fig. 2). Because the Li–Be–B ion intensities were generally low in the CAI

Table 3A
Li, Be, and B concentrations in melilites from Allende 3529-41

Spot #	d[a]	[Li][b]	[Be][b]	[B][b]
I.1[c]	0.21	0.5305	1.2028	0.0970
I.1@1[c]	0.21	0.3607	0.7863	0.0564
I.2[c]	0.37	0.2852	1.4874	0.0670
I.4[c]	0.57	0.1252	0.4749	0.1349
I.5[c]	0.25	0.3040	0.7787	0.9270
I.6[c]	0.37	3.2407	7.5888	0.2790
I.7[c]	0.94	0.0060	2.0604	0.1530
I.7@1[c]	0.94	0.0054	1.6496	0.1382
I.9[c]	0.31	0.4362	0.7892	0.0060
II.5(1)[c]	0.37	0.0149	0.0219	0.3101
II.5(2)[c]	0.37	0.0269	0.0131	0.3338
II.11[c]	0.82	0.0055	0.4363	0.0228
II.13	1.69	0.0220	0.0890	0.0206
II.12bis[c]	0.27	0.1116	0.3437	0.6748
II.12bis@1	0.27	0.3233	0.0348	0.5332
II.15bis	0.45	0.0101	0.0789	0.0244
II.17	0.31	0.0268	0.0749	0.0582
II.18	0.25	0.0139	0.0637	0.0068
III.1-1	0.31	0.0146	0.0960	0.4284
III.1-3[c]	0.62	0.0076	0.1078	0.1272
III.1-4	0.79	0.0161	0.0604	0.0671
III.1-5	0.94	0.0171	0.0749	0.4687
III.1-10[c]	1.50	0.0574	0.2062	0.6783
III.7[c]	0.81	0.0264	0.1478	0.0267
III.8	0.50	0.0115	0.0672	0.0271
III.9[c]	0.60	0.0042	0.0968	0.1599
III.10	0.22	0.0053	0.0485	0.0039
III.11	0.35	0.0189	0.0669	0.0317
III.13(1)[c]	0.12	0.0086	0.1328	0.5259
III.13(2)	0.12	0.4469	0.0252	0.6994
III.15(1)[c]	0.44	0.0035	0.1320	0.0406
III.15(3)[c]	0.44	0.0338	0.0037	0.0595
III.18(1)[c]	0.56	0.0010	0.2811	0.0573
III.18(2)	0.56	0.0336	0.0964	0.0248
III.18(3)	0.56	0.1953	0.0614	0.2589
III.22[c]	0.81	0.0402	0.1673	0.0922
III.23	0.75	0.0267	0.0761	0.0389
III.24[c]	1.37	0.0240	0.1274	0.0174
IV.1	0.31	0.0090	0.0261	0.0045
IV.2	0.22	0.0144	0.0289	0.0017
IV.3	0.44	0.0067	0.0281	0.0040

[a] Distance from the closest edge of the CAI in mm.
[b] Li, Be, and B concentrations are given in ppm. Counting statistics was always better than ±1% relative but uncertainties on ion yields may result in systematic errors up to ±25% relative (see text for details).
[c] Spots where post-magmatic perturbations are suspected (see text and Fig. 4). All analyses correspond to different spots with the exception of spots numbered as "@1" which are duplicates in the same spot and spots numbered (1) or (2) or (3) which correspond to one analysis separated in 2 or 3 data because of the strong heterogeneity of compositions during the course of the sputtering (see text).

Table 3B
Li, Be, and B concentrations in fassaite, anorthite, and the Wark–Lovering rim (bulk) from Allende 3529-41

Spot #	d[a]	[Li][b]	[Be][b]	[B][b]
Fassaite				
I.8	0.44	0.0009	0.0103	0.0330
III.1	0.69	0.0533	0.2194	2.1294
III.2	0.81	0.0158	0.0781	2.0220
III.3(1)[c]	1.06	0.0009	0.0364	0.0591
III.3(2)	1.06	0.0134	0.0284	0.0125
III.5	0.88	0.0010	0.0217	0.0157
III.6	0.94	0.0004	0.0148	0.0420
III.14	0.44	0.0038	0.0081	0.0053
III.17	0.44	0.0025	0.0096	0.0296
III.19(2)	0.53	0.0065	0.0075	0.1929
III.20	1.25	0.0162	0.0255	0.6602
III.21	1.19	0.0033	0.0328	0.3860
Anorthite				
II.1	0.50	0.0013	0.0118	0.2827
II.2[c]	0.63	0.0005	0.0352	0.0140
II.3[c]	0.59	0.0005	0.0344	0.0654
II-6	0.69	0.0441	0.0276	8.6643
II.7(1)	0.46	0.0073	0.0103	0.2325
II.7(2)	0.46	0.0139	0.0112	0.0971
II.8	0.96	0.0080	0.0193	0.0596
II.9	0.96	0.0364	0.0516	0.0046
II.10	0.94	0.0012	0.0045	0.0505
II.10-2[c]	0.0008	0.0349	0.4947	
II.12[c]	0.44	0.0062	0.0878	0.0667
III.1-6	0.81	0.0004	0.0093	0.0678
III.4[c]	0.81	0.0016	0.1445	0.3223
Wark–Lovering rim				
III.12	0.00	0.7893	0.0072	0.3038

[a] Distance from the closest edge of the CAI in mm.
[b] Li, Be, and B concentrations are given in ppm. Counting statistics was always better than ±1% relative but uncertainties on ion yields may result in systematic errors up to ±25% relative (see text for details).
[c] Spots where post-magmatic perturbations are suspected (see text and Fig. 4). All analyses correspond to different spots with the exception of spots numbered as "@1" which are duplicates in the same spot and spots numbered (1) or (2) or (3) which correspond to one analysis separated in 2 or 3 data because of the strong heterogeneity of compositions during the course of the sputtering (see text).

(down to a few counts per second on $^{10}B^+$ for instance), it was not possible to determine concentrations using energy filtering, which might have resulted in better long-term stability for the relative sensitivity factors. However, similar ion yields (3.39 and 2.99 for Li^+/Be^+; 0.389 and 0.394 for B^+/Be^+) were found on the standard glasses during the two sessions in which 3529-41 was analyzed (Table 2). It was assumed that no significant matrix effects on the Li^+/Be^+ and B^+/Be^+ yields exist between silicate glass, anorthite, melilite, and fassaite, though this cannot be demonstrated rigorously from the present set of standards. Although no melilite standard was available, analyses made on various silicates (MORB glasses, olivine, orthopyroxene, clinopyroxene, and feldspar) indicate that matrix effects are not a major source of inaccuracy (Decitre et al., 2002). In fact, the major sources of error on the determination of the $^6Li/^9Be$ and $^{11}B/^9Be$ ratios in 3529-41 are (i) counting statistics and (ii) fluctuations (which often are not correlated) of Li^+ and Be^+ intensities during the course of the measurement. The 2σ errors given in Tables 4A and 4B were calculated from a statistical analysis of the $^6Li/^9Be$ and $^{11}B/^9Be$ ratios in the same way that the errors are calculated for the isotopic ratios. They range from a few percent up to ~25% depending on the Li–Be–B concentrations (Tables 3A and 3B).

In addition to the Li/Be and B/Be ratios, the Li–Be–B concentrations (hereafter referred to as [Li], [Be], and [B])

Table 4A
Li/Be, B/Be ratios, Li and B isotopic compositions of melilites from Allende 3529-41

Spot #	^{9}Be/^{6}Li[a]	^{9}Be/^{11}B[a]	^{7}Li/^{6}Li[a]	^{7}Li/^{6}Li[b]	δ^{7}Li (‰)[b]	^{10}B/^{11}B[a]	δ^{11}B (‰)[a]
I.1[c]	22.63 ± 4.53	18.60 ± 3.72	11.97 ± 0.07	11.97	−3.8 ± 6.0	0.2721 ± 0.0134	−91.6 ± 49.2
I.1@1[c]	21.88 ± 4.38	20.90 ± 4.18	12.04 ± 0.19	12.04	1.9 ± 15.4	0.2712 ± 0.0306	−88.4 ± 112.8
I.2[c]	52.30 ± 10.46	33.30 ± 6.66	12.03 ± 0.09	12.03	1.1 ± 7.2	0.2966 ± 0.0166	−166.5 ± 56.0
I.4[c]	38.03 ± 7.61	5.28 ± 1.06	12.03 ± 0.13	12.03	1.1 ± 11.0	0.2607 ± 0.0082	−51.8 ± 31.4
I.5[c]	25.59 ± 5.12	1.26 ± 0.25	11.98 ± 0.12	11.98	−3.0 ± 10.2	0.2570 ± 0.0042	−38.1 ± 16.2
I.6[c]	23.19 ± 4.64	40.80 ± 8.16	11.88 ± 0.09	11.88	−11.5 ± 7.2	0.2974 ± 0.0214	−168.8 ± 71.8
I.7[c]	3336.95 ± 667.39	20.20 ± 4.04	11.56 ± 0.59	11.64	−31.3 ± 51.0	0.2750 ± 0.0075	−101.3 ± 27.2
I.7@1[c]	2937.02 ± 587.40	17.90 ± 3.58	11.49 ± 0.69	11.57	−37.2 ± 60.2	0.2682 ± 0.0094	−78.3 ± 35
I.9[c]	17.97 ± 3.59	197.30 ± 39.46	11.92 ± 0.07	11.92	−8.5 ± 6.0	0.4189 ± 0.0493	−409.9 ± 117.6
II.5(1)[c]	15.05 ± 0.96	0.11 ± 0.42	11.69 ± 0.14	11.72	−24.7 ± 11.8	0.2529 ± 0.0016	−22.8 ± 6.5
II.5(2)[c]	5.00 ± 0.66	0.06 ± 0.02	9.20 ± 0.22	9.21	−234 ± 24	0.2716 ± 0.0018	−89.8 ± 6.7
II.11[c]	816.15 ± 59.37	28.88 ± 0.26	11.79 ± 0.15	11.88	−11.6 ± 12.3	0.2785 ± 0.0039	−112.5 ± 13.9
II.13	41.62 ± 0.39	6.51 ± 0.01	11.92 ± 0.07	11.94	−6.4 ± 5.9	0.2535 ± 0.0038	−24.8 ± 15
II.12bis[c]	31.66 ± 1.86	0.77 ± 0.71	11.52 ± 0.06	11.52	−41.4 ± 5.4	0.2522 ± 0.0009	−19.9 ± 3.6
II.12bis@1	1.11 ± 0.09	0.10 ± 0.07	11.30 ± 0.03	11.30	−59.7 ± 2.3	0.2545 ± 0.0012	−28.6 ± 4.9
II.15bis	80.65 ± 3.41	4.89 ± 0.18	11.79 ± 0.09	11.84	−14.9 ± 7.9	0.2569 ± 0.0038	−37.9 ± 14.7
II.17	28.70 ± 0.72	1.94 ± 0.01	11.75 ± 0.06	11.77	−20.7 ± 5.2	0.2599 ± 0.0025	−48.8 ± 9.7
II.18	47.13 ± 1.14	14.03 ± 0.19	11.71 ± 0.08	11.74	−23.2 ± 6.6	0.2614 ± 0.0073	−54.5 ± 27.7
III.1-1	67.72 ± 0.60	0.34 ± 0.01	11.84 ± 0.09	11.88	−11.7 ± 8.0	0.2519 ± 0.0013	−18.8 ± 5.1
III.1-3[c]	146.49 ± 3.11	1.28 ± 0.03	11.82 ± 0.15	11.89	−10.9 ± 12.3	0.2523 ± 0.0027	−20.5 ± 10.8
III.1-4	38.52 ± 0.46	1.36 ± 0.05	11.89 ± 0.13	11.92	−8.6 ± 11.1	0.2487 ± 0.0037	−6.0 ± 15.0
III.1-5	45.10 ± 0.56	0.24 ± 0.06	11.90 ± 0.13	11.93	−7.7 ± 10.9	0.2542 ± 0.0015	−27.4 ± 5.8
III.1-10[c]	36.90 ± 10.44	0.46 ± 0.06	11.08 ± 0.10	11.09	−77.6 ± 9.0	0.2548 ± 0.0015	−29.7 ± 5.9
III.7[c]	57.53 ± 0.57	8.34 ± 0.34	11.98 ± 0.11	12.00	−1.7 ± 9.4	0.2479 ± 0.0074	−2.8 ± 29.9
III.8	60.07 ± 0.87	3.73 ± 0.10	12.03 ± 0.16	12.07	4.3 ± 13.7	0.2618 ± 0.0062	−55.9 ± 23.7
III.9[c]	235.70 ± 8.57	0.91 ± 0.03	11.96 ± 0.38	12.08	4.9 ± 31.8	0.2559 ± 0.0040	−34.0 ± 15.7
III.10	94.31 ± 3.48	18.92 ± 1.35	12.22 ± 0.43	12.32	24.9 ± 35.0	0.2850 ± 0.0220	−132.6 ± 77.3
III.11	36.34 ± 0.47	3.19 ± 0.07	11.86 ± 0.16	11.88	−11.3 ± 13.8	0.2611 ± 0.0067	−53.4 ± 25.6
III.13(1)[c]	158.60 ± 32.06	0.38 ± 0.02	11.53 ± 0.18	11.59	−35.8 ± 15.4	0.2555 ± 0.0015	−32.4 ± 5.9
III.13(2)	0.58 ± 0.03	0.054 ± 0.001	11.23 ± 0.04	11.23	−65.7 ± 3.7	0.2598 ± 0.0014	−48.7 ± 5.6
III.15(1)[c]	388.09 ± 36.53	4.91 ± 0.17	11.84 ± 0.16	11.98	−2.8 ± 13.3	0.2570 ± 0.0034	−38.1 ± 13.2
III.15(3)[c]	1.12 ± 0.05	0.09 ± 0.00	11.27 ± 0.11	11.28	−61.5 ± 9.7	0.2610 ± 0.0024	−53.1 ± 9.3
III.18(1)[c]	2806.73 ± 245.39	7.40 ± 0.51	11.72 ± 0.47	12.21	16.2 ± 40.2	0.2578 ± 0.0042	−41.1 ± 16.3
III.18(2)	29.51 ± 1.24	5.85 ± 0.56	11.71 ± 0.09	11.72	−24.7 ± 7.4	0.2609 ± 0.0043	−52.6 ± 16.6
III.18(3)	3.23 ± 1.37	0.36 ± 0.14	10.95 ± 0.12	10.95	−88.9 ± 10.6	0.2585 ± 0.0088	−43.6 ± 34.0
III.22[c]	42.80 ± 2.61	2.74 ± 0.14	11.74 ± 0.06	11.75	−22.5 ± 4.8	0.2529 ± 0.0022	−22.5 ± 8.5
III.23	29.32 ± 0.87	2.95 ± 0.19	11.66 ± 0.05	11.68	−28.3 ± 4.3	0.2547 ± 0.0027	−29.4 ± 10.7
III.24[c]	54.61 ± 1.24	11.08 ± 0.54	11.72 ± 0.05	11.74	−23.4 ± 3.9	0.2601 ± 0.0033	−49.7 ± 12.5
IV.1	29.71 ± 0.47	8.84 ± 0.37	11.79 ± 0.14	11.85	−14.4 ± 12.1	0.2603 ± 0.0140	−50.5 ± 53.6
IV.2	20.67 ± 0.32	25.18 ± 2.87	11.69 ± 0.15	11.72	−25.0 ± 13.1	0.2785 ± 0.0190	−112.5 ± 68.2
IV.3	42.94 ± 1.06	10.47 ± 0.66	11.83 ± 0.10	11.90	−9.9 ± 8.2	0.2628 ± 0.0094	−59.3 ± 35.7

[a] Errors are 2σ.
[b] Li isotopic composition corrected for the amount of ^{6}Li, ^{7}Li, and ^{7}Be produced during GCR irradiation of the Allende meteoroid (see text for details).
[c] Spots where post-magmatic perturbations are suspected (see text and Fig. 4).

were determined by comparison between sample and standards of the Li–Be–B intensities normalized to the primary beam intensities. This approach was chosen, instead of measuring Li–Be–B relative to a matrix ion such as Si^{+}, in order to maximize the counting time on the Li–Be–B peaks and to avoid possible instabilities of the magnetic field when commuting from Si to Li. This assumes that not only relative ion yields of Li–Be–B are matrix independent, but also that absolute sputter yields (secondary ions/primary ion) are constant. Given that the phases under investigation are all silicates, this assumption is reasonable and the absolute concentration measurements are probably accurate to better than 25%. The Li–Be–B concentrations are given in ppm in Tables 3A and 3B. The errors are not given in Tables 3A and 3B because they are low (always less than a few percent relative, not considering possible systematic uncertainties). These errors depend on the counting statistics and possibly on changes in ion emissivity due to variations in parameters such as charging (quality of coating) or surface exposed to the primary beam (presence of cracks or not, surface roughness, etc.). Though the variation of these latter parameters cannot be determined precisely for each spot, the quality of polishing of the section was good and the sample was re-coated several times to maintain charging effects at a minimum. Even in cases where counting statistics are the overall limiting factor, e.g., for minerals with very low Li–Be–B concentrations, the uncertainties on concentration measurements are quite good: taking, for example, spot II-2 in anorthite (see Table 3B) which has amongst the lowest [Li] = 0.5 ppb

Table 4B
Li/Be, B/Be ratios, Li and B isotopic compositions of fassaite, anorthite, spinel, and the Wark–Lovering rim (bulk) from Allende 3529-41

Spot #	$^{9}Be/^{6}Li$[a]	$^{9}Be/^{11}B$[a]	$^{7}Li/^{6}Li$[a]	$^{7}Li/^{6}Li$[b]	$\delta^{7}Li$ (‰)[b]	$^{10}B/^{11}B$[a]	$\delta^{11}B$ (‰)[a]
Fassaite							
I.8	115.29 ± 21.57	0.470 ± 0.094	11.47 ± 0.72	12.01	−1.1 ± 63.0	0.2513 ± 0.0075	−16.3 ± 29.8
III.1	42.31 ± 9.32	0.155 ± 0.023	11.86 ± 0.13	11.86	−12.9 ± 10.6	0.2516 ± 0.0019	−17.4 ± 7.7
III.2	50.69 ± 13.42	0.058 ± 0.002	11.80 ± 0.18	11.83	−15.6 ± 14.9	0.2486 ± 0.0013	−5.6 ± 5.3
III.3(1)[c]	437.11 ± 47.84	0.929 ± 0.047	11.23 ± 0.28	11.77	−20.4 ± 25.0	0.2543 ± 0.0029	−27.9 ± 11.3
III.3(2)	21.87 ± 2.24	3.428 ± 0.272	12.09 ± 0.13	12.13	9.2 ± 11.1	0.2574 ± 0.0068	−39.8 ± 26.3
III.5	229.18 ± 14.29	2.087 ± 0.062	12.20 ± 0.66	12.77	62.6 ± 54.3	0.2359 ± 0.0110	48.0 ± 46.7
III.6	388.59 ± 23.48	0.532 ± 0.014	11.99 ± 0.82	13.46	120.1 ± 68.2	0.2468 ± 0.0057	1.4 ± 23.1
III.14	22.12 ± 1.62	2.312 ± 0.202	11.64 ± 0.13	11.77	−20.6 ± 11.5	0.2628 ± 0.0099	−59.3 ± 37.5
III.17	38.95 ± 3.60	0.490 ± 0.023	11.68 ± 0.18	11.88	−11.8 ± 15.4	0.2499 ± 0.0033	−10.7 ± 13.3
III.19(2)	11.80 ± 2.24	0.058 ± 0.005	11.25 ± 0.79	11.32	−58.1 ± 70.2	0.2548 ± 0.0036	−29.8 ± 14.0
III.20	16.21 ± 3.11	0.058 ± 0.003	11.55 ± 0.13	11.58	−36.5 ± 11.4	0.2521 ± 0.0017	−19.3 ± 6.6
III.21	103.19 ± 22.24	0.128 ± 0.017	11.60 ± 0.15	11.75	−22.7 ± 13.1	0.2553 ± 0.0019	−31.9 ± 7.4
Anorthite							
II.1	91.93 ± 4.07	0.063 ± 0.001	11.30 ± 0.37	11.65	−30.6 ± 32.6	0.2538 ± 0.0018	−26.1 ± 7.0
II.2[c]	737.81 ± 49.02	3.795 ± 0.001	10.99 ± 0.60	11.94	−6.9 ± 54.2	0.2680 ± 0.0069	−77.7 ± 25.9
II.3[c]	664.49 ± 48.06	0.792 ± 0.000	10.77 ± 0.34	11.60	−35.0 ± 31.5	0.2498 ± 0.0021	−10.5 ± 8.4
II-6	6.43 ± 0.40	0.005 ± 0.000	11.44 ± 0.07	11.45	−47.5 ± 5.7	0.2545 ± 0.0006	−28.7 ± 2.3
II.7(1)	14.51 ± 1.50	0.067 ± 0.016	10.41 ± 0.23	10.46	−129.6 ± 22.3	0.2626 ± 0.0028	−58.6 ± 10.7
II.7(2)	8.26 ± 0.25	0.173 ± 0.005	11.57 ± 0.12	11.61	−34.1 ± 10.0	0.2511 ± 0.0023	−15.6 ± 9.3
II.8	24.93 ± 1.62	0.489 ± 0.000	11.70 ± 0.13	11.77	−21.1 ± 11.0	0.2559 ± 0.0026	−34.0 ± 10.2
II.9	14.60 ± 0.19	17.024 ± 0.004	11.77 ± 0.06	11.79	−19.2 ± 4.7	0.2629 ± 0.0099	−59.9 ± 37.6
II.10	38.78 ± 2.51	0.134 ± 0.007	11.62 ± 0.26	12.03	1.2 ± 22.6	0.2590 ± 0.0027	−45.6 ± 10.5
II.10-2[c]	436.11 ± 1.50	0.106 ± 0.007	11.49 ± 0.40	12.09	5.6 ± 34.7	0.2562 ± 0.0011	−35.1 ± 4.1
II.12[c]	145.25 ± 9.99	1.986 ± 0.010	11.80 ± 0.12	11.88	−11.8 ± 10.2	0.2553 ± 0.0022	−31.9 ± 8.6
III.1-6	266.64 ± 12.55	0.206 ± 0.007	11.84 ± 0.56	13.44	117.9 ± 47.2	0.2498 ± 0.0001	−10.5 ± 0.2
III.4[c]	942.93 ± 174.45	0.676 ± 0.039	11.91 ± 0.57	12.24	18.1 ± 48.2	0.2522 ± 0.0031	−20.0 ± 12.4
Spinel (cluster of spinel grains in melilite)							
I.3	2.52 ± 0.50	0.49 ± 0.10	12.12 ± 0.09	n.d.	8.5 ± 7.4	0.2533 ± 0.0046	−24.2 ± 18.0
Wark–Lovering rim							
III.12	0.093 ± 0.002	0.036 ± 0.003	11.60 ± 0.04	11.60	−34.5 ± 3.5	0.2548 ± 0.0011	−30.1 ± 4.5

[a] Errors are 2σ.
[b] Li isotopic composition corrected for the amount of ^{6}Li, ^{7}Li, and ^{7}Be produced during GCR irradiation of the Allende meteoroid (see text for details).
[c] Spots where post-magmatic perturbations are suspected (see text and Fig. 4).

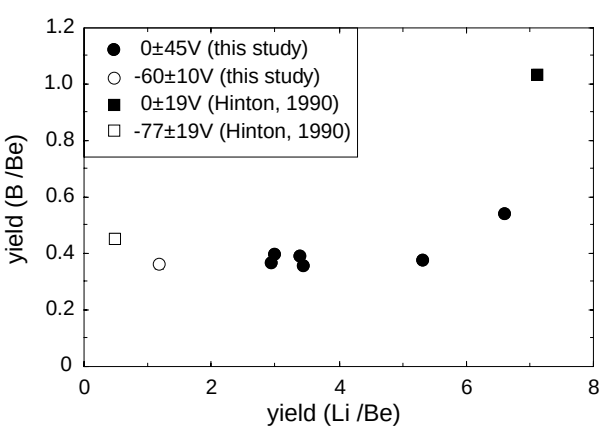

Fig. 2. Variations with secondary ion energies of Li, and B ion yields relative to Be (see above-mentioned reference for further information).

and which was sputtered with a 40 nA primary beam, the average count rate on $^{7}Li^{+}$ was 0.46 counts/s/nA, which corresponds to a total number of 7360 $^{7}Li^{+}$ ions counted (for 100 cycles), implying a 2σ counting error of ±2.3% relative.

Instrumental mass fractionation, inherent in SIMS, was corrected by comparison to analyses of the GB4 glass standard made under the same analytical conditions (with low primary beam intensity). The reproducibility of Li and B isotopic analyses on this glass is generally of the order of ±2‰ (see Table 2). As generally observed for Li isotope analyses, the Li instrumental mass fractionation (defined as $\alpha_{inst}(Li) = (^{7}Li/^{6}Li)_{true}/(^{7}Li/^{6}Li)_{measured}$) was >1. This behavior is contrary to those of other elements, almost all of which exhibit mass fractionation in SIMS favoring the lighter isotopes. The theoretical reason for this is not understood, but it is always observed when settings of the electron multiplier (high voltage and threshold) are correct and, additionally, values of α_{inst} for Li and B appear to be broadly positively correlated (Chaussidon et al., 1997; Fig. 3). Previous experience has shown that matrix effects on the instrumental mass fractionation are not a serious complication for silicate minerals (Beck et al., 2004; Decitre et al., 2002) and thus the use of GB4 glass to correct for α_{inst} for analyses made on melilite, fassaite, and anorthite should result in accurate measurements within the stated precision. The corrected Li and B isotopic compositions

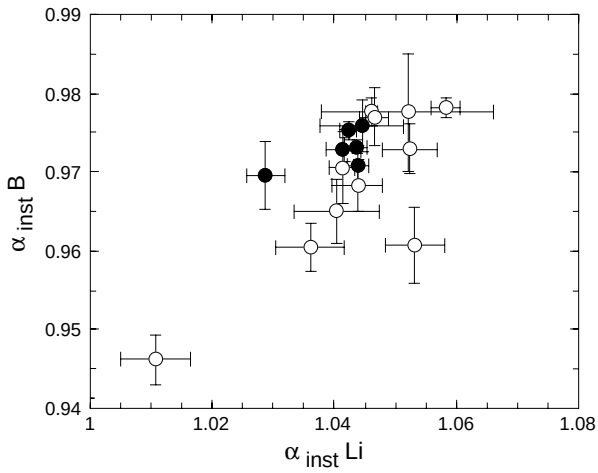

Fig. 3. Li and B instrumental mass fractionations (see text for definition of α_{inst}) during ion probe isotopic analyses. Note that α_{inst} is >1 for Li.

are given in Tables 4A and 4B either as ^{7}Li/^{6}Li and ^{10}B/^{11}B ratios or in delta notation, δ^{7}Li (relative to L-SVEC with ^{7}Li/^{6}Li = 12.0192) for Li, and δ^{11}B (relative to NBS 951 with ^{11}B/^{10}B = 4.04558) for B. Two sigma errors on the Li and B isotopic compositions are given in Tables 4A and 4B. These errors are always much higher than the reproducibility of the determinations of α_{inst} on the Li- and B-rich glass standard, which is thus not the limiting factor in the precision of the Li and B isotopic analyses of CAIs.

3. Results

3.1. Li–Be–B distributions in Allende CAI 3529-41

The absolute Li–Be–B concentrations ([Li], [Be], and [B], respectively), as well as those of Be/Li and Be/B are highly variable on small spatial scales in 3529-41 (Tables 3A, 3B and 4A, and 4B). The ^{9}Be/^{6}Li ratios range from 0.6 to 3337 in melilite, from 11.8 to 437.1 in fassaite, and from 6.4 to 942.9 in anorthite. The ^{9}Be/^{11}B ratios range from 0.1 to 197.3 in melilite, from 0.06 to 3.4 in fassaite, and from 0.005 to 17.2 in anorthite. Clearly the largest fractionation of B relative to Be is observed in melilite while the three major mineral phases show variable fractionation of Li relative to Be. Average Li–Be–B concentrations show that fassaite and anorthite are significantly depleted in Li and Be relative to melilite: average [Li] and [Be] are 0.168 and 0.491 ppm in melilite, but only 0.010 and 0.040 ppm in fassaite, and 0.010 and 0.037 ppm in anorthite, respectively. On the other hand, average boron concentrations are rather similar in all three phases: [B] = 0.188 ppm in melilite, 0.140 ppm in fassaite, and 0.155 ppm in anorthite. No systematic distribution is observed between the location in the CAI and Li–Be–B concentrations: Li- and B-poor spots can be found either in the melilite-rich rim of the CAI or in the spinel-rich core. However, it is notable that the spot from the Wark–Lovering rim shows significantly higher [Li] and [B] (0.783 and 0.303 ppm, respectively) than the bulk of the CAI, but it has a low [Be] = 0.007 ppm.

Previous Li–Be–B concentration data in CAIs are scarce but they show similar features to what we observed in 3529-41. For instance, Phinney et al. (1979) reported for Allende CAI EK-1-07 [Li] = 0.244–0.340 ppm in melilite, 0.066 ppm in fassaite, and 0.070 ppm in anorthite, with [Be] = 0.429 ppm in melilite, 0.177 ppm in fassaite, and 0.127 ppm in anorthite. The [B] of EK-1-07 was found to be much higher for all phases (from 1.4 to 2.0 ppm) than in 3529-41. A similar situation was observed for Allende USNM 3515 (Chaussidon et al., 2002) and is most likely related to the introduction of B in the CAI during some alteration or possibly during polishing and sample preparation. In fact, the [B] in CAIs appears to be extremely variable from one inclusion to another: Sugiura et al. (2001) found [B] ranging from 0.004 to 0.1 ppm in 4 CAIs from Efremovka and two from Allende, while MacPherson et al. (2003) found [B] ranging from 0.00009 to 0.087 ppm (most of the data being around a few ppb) in 7 CAIs from Efremovka, Vigarano, Leoville, and Allende. Spivack et al. (1987) reported [Be] for two Allende CAIs ranging from 0.050 to 0.150 ppm in melilite and bulk [Be] for 9 Allende CAIs ranging from 0.150 to 0.570 ppm. These latter data are in very good agreement with our measurements in 3529-41.

3.2. Li and B isotopic variations in Allende CAI 3529-41

3.2.1. Range of variations of ^{7}Li/^{6}Li and ^{10}B/^{11}B

The Li and B isotopic compositions are given in Tables 4A and 4B. They both show a large range of variations from 9.20 ± 0.22 to 12.22 ± 0.43 for ^{7}Li/^{6}Li ratios (i.e., δ^{7}Li ranging from −235 to +15‰) and from 0.2468 ± 0.0057 to 0.4189 ± 0.0493 for ^{10}B/^{11}B (i.e., δ^{11}B ranging from −410 to +4‰). The ^{7}Li/^{6}Li ratio of 9.20 ± 0.22 is the lowest one ever found in CAIs, the second lowest ratio being 9.9 ± 1.1 found in Axtell CAI 2771 (MacPherson et al., 2003). ^{7}Li/^{6}Li ratios much lower than chondritic, similar to those found in 3529-41, have been previously observed in CAIs (Chaussidon et al., 2002; MacPherson et al., 2003; Phinney et al., 1979). There is no systematic difference in isotopic composition between the different mineral phases in 3529-41. Mean ^{7}Li/^{6}Li and ^{10}B/^{11}B ratios are, respectively, 11.68 ± 0.48 and 0.2661 ± 0.0270 for melilite, 11.67 ± 0.31 and 0.2550 ± 0.0066 for fassaite, and 11.57 ± 0.45 and 0.2561 ± 0.0055 for anorthite. On average, 3529-41 appears slightly depleted in ^{7}Li and ^{11}B relative to chondrites, by ≈30‰ for Li and ≈40‰ for B. These average δ^{7}Li and δ^{11}B values (−30 and −40‰, respectively) correspond to the lowest values found in chondrules (Chaussidon and Robert, 1998; Robert and Chaussidon, 2003). The analysis made on the Wark–Lovering rim of 3529-41 shows Li and B isotopic compositions similar to the average CAI (δ^{7}Li = −34 ± 3% and δ^{11}B = −30 ± 5‰). There is no apparent correlation

between the Li and B isotopic ratio and their geographic distribution in the CAI. The only noticeable trend is a rather systematic decrease of $^{7}Li/^{6}Li$ ratio in phases with very low [Li] (probably due to recent irradiation of the Allende meteroid, see next section). Finally, it is important to note that in some cases large isotopic variations are observed at a few hundreds micrometer scale.

3.2.2. Corrections for GCR exposure of the Allende meteoroid

Because some mineral phases in 3529-41 (exclusively fassaite and anorthite) have extremely low [Li], below the ppb level, the contribution of spallogenic Li produced during the recent exposure of the Allende meteoroid to GCR in the interplanetary space must be considered. Studies of cosmogenic noble gases have shown that the Allende meteoroid had a pre-atmospheric radius of ≈60 cm (Bourot-Denise and Pellas, 1982) and had been exposed to GCR as a small body for 5.2 ± 0.3 Ma (Fireman and Goebel, 1970). This GCR exposure age is in the middle of the range found for CV3 chondrites which varies from ~2 to 35 Ma (Scherer and Schultz, 2000).

The production in meteorites of spallogenic elements from the interaction with GCR is a difficult process to model because most of the spallation products are not due to collisions with primary protons but to collisions with secondary protons and neutrons. This was recently studied experimentally for cosmogenic ^{10}Be and ^{26}Al by irradiation with 1.9 GeV protons of targets of chondritic compositions (Michel et al., 1996). Based on these data, Leya et al. (2000a) developed a model which reproduces the absolute level and the variations with depth of spallogenic ^{10}Be and ^{26}Al activities observed in several chondrites for which the precise estimates of the pre-atmospheric size and shape have been constructed. The production rates of ^{10}Be have been tabulated as a function of the chemical composition of the meteoroid for a total GCR flux of 4.06 nucleons $cm^{-2}\,s^{-1}$ with energy >10 MeV (Leya et al., 2000a). A minimum production rate of $^{10}Be \approx 15$ atoms $mn^{-1}\,kg^{-1}$ is calculated for a CAI in a meteoroid of 60 cm radius (it depends slightly on the depth of the CAI in the meteoroid but cannot be lower than 15 and higher than 20). For an exposure age of 5.2 Ma, this translates into 4.1×10^{13} atoms kg^{-1} of ^{10}Be produced.

Spallogenic Li includes both ^{6}Li and ^{7}Li with ^{7}Li produced primarily by the radioactive decay of spallogenic ^{7}Be. No calculation similar to that shown above for ^{10}Be exists for the production of ^{7}Be, ^{6}Li, and ^{7}Li, but some irradiation experiments have been done to determine the production rate of ^{7}Be in an artificial chondrite at 1.6 GeV (Leya et al., 2000b). The amount of spallogenic ^{7}Be, ^{6}Li, and ^{7}Li produced by GCR in Allende can be estimated by scaling the production rate of ^{10}Be using the ratio of the known cross-sections for the production by protons on O nuclei of ^{6}Li, ^{7}Li, and ^{7}Be relative to ^{10}Be at 650 MeV. Available values for these cross-sections are 1.52 ± 0.15 mb for ^{10}Be, 11.3 ± 0.8 mb for ^{7}Be, 12.4 ± 2.4 mb for ^{6}Li, and 11.3 ± 2.2 mb for ^{7}Li (Michel et al., 1989; Read and Viola, 1984). This gives a total spallogenic production in an Allende CAI of 3.34×10^{14} atoms kg^{-1} of ^{6}Li (i.e., $4.1 \times 10^{13} \times 12.4/1.52$) and 6.10×10^{14} atoms kg^{-1} of ^{7}Li (i.e., $4.1 \times 10^{13} \times (11.3 + 11.3)/1.52$). Because the $^{7}Li/^{6}Li$ ratio of this spallogenic Li is ≈1.83, corrections for it will inevitably increase the calculated $^{7}Li/^{6}Li$ ratios in 3529-41 prior to recent GCR exposure. While this correction is negligible for high [Li] (e.g., a $^{7}Li/^{6}Li$ ratio of 11.5 is increased after correction by only 0.4‰ in a spot having a [Li] of 0.1 ppm), it is rather significant for extremely low [Li] (e.g., a $^{7}Li/^{6}Li$ ratio of 11.5 in a spot having a [Li] of 0.0005 ppm is increased after correction by 90‰). In the following discussion, the $^{7}Li/^{6}Li$ ratios in 3529-41 (Tables 4A and 4B) have been corrected for the interaction with GCR according to procedures outlined here. Finally, note that GCR irradiation has no significant effect on B isotopic compositions because of the higher B abundances relative to Li in 3529-41.

4. Discussion

4.1. Processes controlling the Li–Be–B distributions in Allende CAI 3529-41

The major difficulty in searching for traces of the in situ decay of radioactive ^{7}Be and ^{10}Be in CAIs, apart from the generally low Li–Be–B concentrations, is that the "pristine" Li–Be–B distributions and/or Li and B isotopic compositions may have been disturbed locally by secondary processes. That such processes have occurred generally in Allende CAIs and in 3529-41 in particular is demonstrated convincingly by the numerous disturbances of the $^{26}Al/^{26}Mg$ system, especially in melilite, documented by Podosek et al. (1991). In addition, it seems very likely that, contrary to Be, most of the Li present in the CAI is not inherited from high temperature condensation processes but was introduced into the CAI at a later stage and redistributed during re-melting events. This is in keeping with the more refractory nature of Be compared to either Li or B. Thermodynamic equilibrium calculations estimate that 50% of Be will condense at 1500 K either as gugaïte ($Ca_2BeSi_2O_7$) in solid solution with melilite or into spinel. On the other hand, the 50% condensation temperature of B is only 964 K where it is incorporated mostly as danburite ($NaBSi_3O_8$) in solid solution with anorthite (Lauretta and Lodders, 1997). The thermodynamic behavior of Li is intermediate with a predicted 50% condensation temperature of 1225 K (Wai and Wasson, 1977). Thus, it appears that the very low concentration levels (ppb to ppm range) of Li and B, primarily in fassaite and anorthite, reflect the moderately volatile nature of these elements compared to the high condensation temperatures characteristic of major CAI minerals, whereas more refractory Be is enhanced relative to chondritic values. Additionally, the large range of [Li] and, to a lesser extent [B], observed in 3529-41 indicates that a significant fraction of Li must have been

introduced into the CAI at a later time, i.e., after gas–solid condensation of its precursor minerals.

This problem of the presence of moderately volatile elements in CAIs has been addressed in great detail for Na which has a condensation temperature similar to that of B. The mineral partitioning of Na has been investigated experimentally (Beckett and Stolper, 2000) and its distribution in CAIs has been analyzed both at the crystal scale and at the inclusion scale in many samples (Beckett et al., 2000 and references therein). A number of hypotheses (summarized in Beckett et al., 2000) have been proposed to explain the observations that, despite the relatively volatile nature of Na, high Na_2O contents are observed in melilite (often >0.05 wt%) and melilite Na_2O contents often correlate with Åk content in a way suggesting a control by partitioning between melilite and melt. One possibility could be that after initial crystallization of the CAI, a large fraction (or all) of the Na is introduced into the CAI during low temperature alteration in the nebula and is then re-distributed in the CAI through re-melting and melilite crystal fractionation possibly (depending on cooling rate) followed by a relaxation of concentration gradients by diffusion. In principle, this scenario may be repeated through a succession of re-melting events. Similar processes could be called upon to explain the presence of Li and B in CAIs.

In the following, we investigate whether similar secondary processes could help explain the large range of Li–Be–B concentrations observed in 3529-41. The goal is to find whether any relationships could be expected with either major element compositions of the main mineral phases or the geographic distribution of the analytical spots in the CAI that might help distinguish "primary" signatures from those overprinted by secondary processes. Identifying (among the different analytical spots) those zones where the Li and Be distributions were altered by secondary processes is especially crucial in the case of the ^{7}Be/^{7}Li system because of the very short half-life of ^{7}Be (53 days) which makes this system very sensitive to post-magmatic processes.

4.1.1. Traces in 3529-41 of Li–Be partitioning during magmatic processes

Some simple criteria can be worked out to test whether the Be distribution in the three major mineral phases of the CAI (melilite, anorthite, and fassaite) is inherited from magmatic processes or not. For melilite, the partitioning of Be between crystal and melt has been investigated experimentally (Beckett et al., 1990). Be appears to be moderately incompatible in gehlenitic melilites with $D_{\text{melilite/melt}} = 0.5$ for $X_{\text{Åk}} = 0.3$ and compatible in akermanitic melilites with $D_{\text{melilite/melt}} = 1.9$ for $X_{\text{Åk}} = 0.75$. This variation of the partition coefficient with melilite composition (determined with an uncertainty of ±20% relative, Beckett et al., 1990) allows one to predict the magnitude of increase of Be concentration in melilite as a function of its composition ($X_{\text{Åk}}$), assuming only closed-system crystal fractionation of melilite (Beckett et al., 1990). Fig. 4 shows, in a diagram

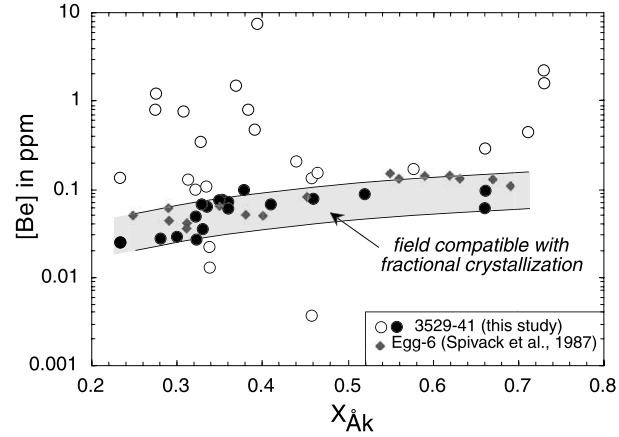

Fig. 4. Variations of Be concentrations in melilites versus Åkermanite contents in CAI 3529-41. The light gray field corresponds to the range of [Be] compatible with closed-system crystal fractionation of a CAI melt (see text for details). The melilite spots have been divided in two groups: one (closed dots) corresponding to melilite compositions compatible with closed-system crystal fractionation and another one (open dots) corresponding to melilites whose [Be] cannot be explained by fractionation during magmatic differentiation of the CAI melt. Closed diamonds represent [Be] determined for another Allende CAI, Egg-6 (Spivack et al., 1987), and used to validate models based on experimental determination of Be partition coefficients between melilite and melt (Beckett et al., 1990).

[Be] versus melilite composition ($X_{\text{Åk}}$), a comparison between the predicted crystal fractionation trends and data for Allende CAI Egg-6 (analyses on melilite separates by Spivack et al., 1987) and Allende 3529-41 (this study). Two extreme trends were calculated for the [Be] range of initial CAI liquids corresponding to the composition of the melilites with the lowest [Be] and lowest $X_{\text{Åk}}$: i.e., $0.02\ \text{ppm} < [\text{Be}]_{\text{melilite}} < 0.05\ \text{ppm}$ for $0.28 < X_{\text{Åk}} < 0.32$ (four spots in melilite used: III-10, IV-1, IV-2, and IV-3, see Tables 1A and 3A). This corresponds to a range of [Be] in CAI liquid from ≈0.03 to ≈0.09 ppm: such a factor of 3 uncertainty allows one to maximize within realistic limits the range of [Be] that can be predicted for melilite crystallized from an initially homogeneous CAI melt. The same approach was used in Beckett et al. (1990) to compare the data on Egg-6 (Spivack et al., 1987) with experimental predictions. Egg-6 melilite shows $[\text{Be}] \approx 0.05$ ppm with $X_{\text{Åk}} = 0.25$, which is within the range measured in 3529-41. It is obvious from Fig. 4 that many spots show higher [Be], by up to one order of magnitude, relative to the [Be] that can be reached during melilite crystal fractionation in a CAI melt (these spots have been identified by open dots in Fig. 4). Similarly, a small fraction of spots show a significantly lower [Be] than would be predicted from mineral–melt partitioning. Thus, only a fraction (18 spots over 41, closed dots in Fig. 4) of the analytical spots in 3529-41 corresponds to melilite having [Be] consistent with crystal fractionation in a closed system. These melilite spots are hereafter referred to as "magmatic trend" melilites.

Some of the melilite spots are rather close to the magmatic range defined in Fig. 4 but because they are outside this range they are logically considered as perturbed for

purposes of the following discussion. Note, however, that their "rejection" will not quantitatively affect the discussion concerning the possible presence of ^{7}Li excesses due to the in situ decay of ^{7}Be. For example, consider points III.22 ($X_{\mathring{A}k} = 0.56$ and [Be] = 0.17 ppm) and II.5(1) ($X_{\mathring{A}k} = 0.34$ and [Be] = 0.0219) which are the closest to the magmatic range we defined; these points, though rejected, would, however, plot within errors on the ^{7}Be isochron shown in Fig. 10. On the other hand, point III.1-1 ($X_{\mathring{A}k} = 0.38$ and [Be] = 0.096 ppm) is just touching the magmatic trend in Fig. 4 and therefore was considered as non-perturbed; however, inclusion of this point does not strongly constrain the ^{7}Be isochron.

No experimental data exist for the Li partition coefficient between melilite and melt ($D^{Li}_{melilite-melt}$), but the increase of [Li] in the "magmatic trend" melilites (from ≈0.01 to ≈0.03 ppm, with one spot having an extreme [Li] of 0.19 ppm, Table 3B) seems grossly consistent with crystal fractionation in closed system (Fig. 6A). For example, a constant $D^{Li}_{melilite-melt}$ of 0.1 would predict a factor of 1.5 increase of the [Li] from $X_{\mathring{A}k} = 0.25$ to $X_{\mathring{A}k} = 0.70$. However, it may not be possible to construct such a petrologic model for [Li] because, as previously mentioned, Li is not refractory whereas Be is. Thus, it is likely that Li was introduced in the CAI by alteration and localized re-melting in the nebula, and it is not possible to derive a specific [Li] for the CAI melt at any one time in its history. In general, the spots belonging to the "magmatic trend" have, in average, lower [Li] (0.067 ppm), [Be] (0.061 ppm), and [B] (0.15 ppm) than the others. The processes possibly responsible for the variations of [Be] and [Li] in the other 23 melilite spots (hereafter referred to as "non-magmatic melilite spots") are discussed in the following section.

In contrast to the situation for melilite, partitioning experiments are lacking with which to model the evolution of Li and Be concentrations in fassaite and anorthite during crystal fractionation of a CAI melt. However, some partitioning data obtained for terrestrial mantle rocks do exist for feldspar and pyroxene. Li and Be are both incompatible in plagioclase with $D^{Li}_{plag-melt} = 0.22 \pm 0.01$ and $D^{Be}_{plag-melt} = 0.27 \pm 0.06$ (Ryan and Langmuir, 1987, 1988) and in pyroxene as well with $D^{Li}_{px-melt}$ ranging from 0.14 to 0.27 and $D^{Be}_{px-melt}$ ranging from 0.0025 to 0.021 (Brenan et al., 1998; Herd et al., 2004). On the basis of these partition coefficients it can be predicted that Li and Be concentrations of anorthite and fassaite must increase together during crystal fractionation. In Fig. 5, the Li and Be concentrations of anorthite and fassaite are compared with four fractionation trends calculated for extreme starting compositions of the CAI melt ranging from 0.005 to 0.06 ppm for Li and from 0.03 to 0.1 ppm for Be (see Fig. 5 caption for details). In fact, some anorthite and fassaite crystals are observed in 3529-41 to be present as inclusions in the melilite-rich mantle (and thus to be rather early in the crystallization sequence), while most of them are in the spinel-rich core and thus likely crystallized after

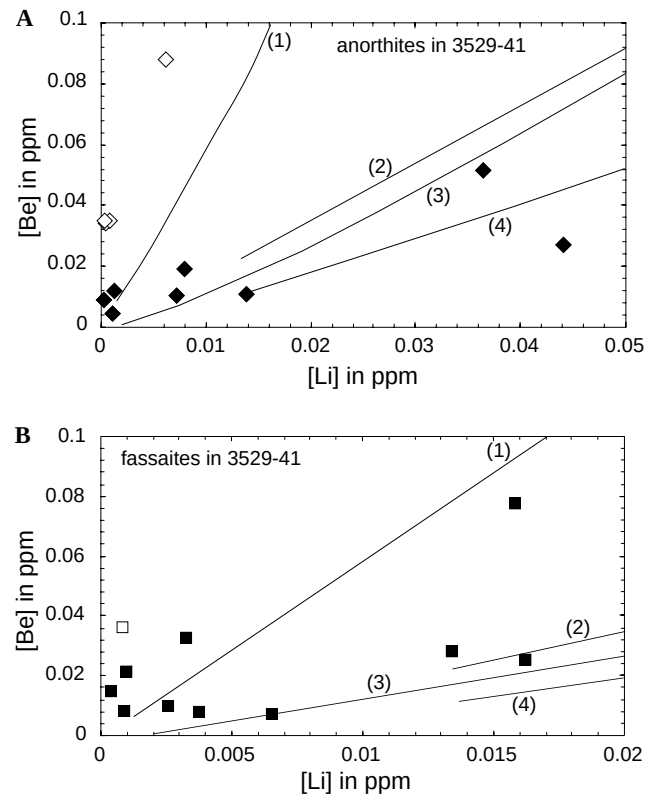

Fig. 5. Variations of Be versus Li concentrations in anorthites (A) and fassaites (B) from CAI 3529-41. Four trends of closed-system crystal fractionation were calculated assuming an extreme range of initial Li and Be concentration (noted $[Li]_0$ and $[Be]_0$) of the CAI and of Li and Be partition coefficients between crystal and melt (see text for details): $[Li]_0 = 0.005$ ppm, $[Be]_0 = 0.05$ ppm, $D^{Li} = 0.27$ and $D^{Be} = 0.23$ for (1); $[Li]_0 = 0.05$ ppm, $[Be]_0 = 0.1$ ppm, $D^{Li} = 0.27$ and $D^{Be} = 0.23$ for (2); $[Li]_0 = 0.01$ ppm, $[Be]_0 = 0.1$ ppm, $D^{Li} = 0.2$ and $D^{Be} = 0.016$ for (3); and $[Li]_0 = 0.06$ ppm, $[Be]_0 = 0.1$ ppm, $D^{Li} = 0.27$ and $D^{Be} = 0.12$ for (4). Five spots in anorthites and one in fassaite (open symbols) have Be–Li concentrations incompatible with closed-system crystal fractionation (see text for discussion).

most of the CAI melilite was crystallized. The starting compositions for the CAI melt were thus chosen to cover the possible range from concentrations at equilibrium with the lowest [Li] and [Be] in anorthite and fassaite to concentrations corresponding to melt at equilibrium with late melilite (e.g., $[Be]_{melt} = 0.1$ ppm corresponds to a melilite with $X_{\mathring{A}k} = 0.6$ containing 0.13 ppm of Be since $D^{Be}_{melilite-melt} = 1.35$ for this composition). The comparison between calculated trends and the data permits the identification of five spots in anorthite for which a huge increase of [Be] is observed with no associated increase in [Li] (Fig. 5A). As with the melilites exhibiting high [Be] with low [Li] in Fig. 4, the Li–Be distributions in these anorthite grains cannot be explained by closed-system crystal fractionation. Only one fassaite crystal shows a significant [Be] increase not associated with a commensurate increase in [Li] (Fig. 5B).

In conclusion, the Li and Be distributions in melilite, anorthite, and fassaite reveal that for a number of analytical

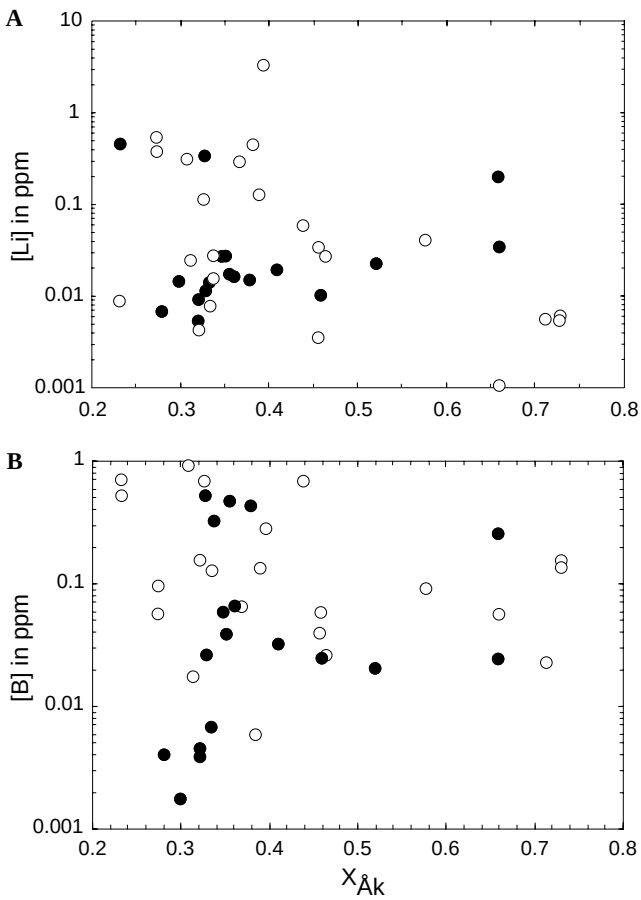

Fig. 6. Variations of Li (A) and B (B) concentrations in 3529-41 melilite versus Åkermanite contents (symbols are the same as in Fig. 4). Contrary to [Be] in Fig. 4, there is no clear relationship between [Li] or [B] and $X_{Åk}$, implying that lithium and boron concentrations reflect mostly post-magmatic perturbations.

spots (23 over 41 in melilite, 5 over 13 in anorthite, and 1 over 12 in fassaite) the [Li] and [Be] are not compatible with crystal fractionation in a closed system. These points show obvious signs of a redistribution of Li and/or Be after the last magmatic event as recorded, for instance, in the Åk content of melilites. Applying similar criteria to Li and B concentrations shows that there is no clear correlation between [Li], [B], and $X_{Åk}$ in melilite or the other phases as well (Figs. 6A and B). Most of the B distribution appears to have been perturbed by post-magmatic events.

4.1.2. Origin of the "non-magmatic" Li–Be distributions in 3529-41

The points in which the Li and/or Be distributions have been perturbed by secondary processes are obviously not the most interesting ones for the search of traces of in situ ^{7}Be decay, so processes possibly responsible for these perturbations are only briefly discussed here. Although considered relatively pristine by Allende standards, CAI 3529-41, nevertheless, shows evidence of significant mineralogic alteration with, for instance, secondary grossular and anorthite (Podosek et al., 1991). Zones and veins of altered melilite are present in 3529-41 as typically observed in Allende type B CAIs (MacPherson et al., 1988), melilite being probably the mineral the most easily altered (Brearley and Jones, 1998). Not surprisingly then, it is predominantly in melilite in 3529-41 where there is a higher proportion of spots showing perturbed Li–Be distributions relative to the calculated primary magmatic distributions: 56% in melilite compared to 38% in anorthite and only 8% in fassaite. During ion probe analyses, efforts were made to avoid zones where cracks or signs of obvious alteration were present. However, because the size of the primary O^- beam had to be large (~50–80 μm in diameter) and the sputtered crater relatively deep (a few microns) in order to minimize surficial contamination and get enough counts on Li–Be–B, it is not surprising that in many cases alteration phases were sputtered together with unaltered phases. One might speculate that spinel would show the least susceptibility to alteration (e.g., in analogy with oxygen isotope distributions), however, all spinels are too small to be analyzed as individual phases under these experimental conditions. Similar to petrographic studies of alteration in CAIs, no clear systematic relationship is observed between the geographic distribution of the spots in the CAI and the presence of alteration products in them.

Two obvious signs of this "mixing problem" under the ion probe beam were observed. First, an abrupt change of the Li–Be–B intensities during the ion probe measurements occurred in a few cases, which resulted in a strong change of up to two orders of magnitude of the ^{9}Be/^{6}Li ratio for instance. This was the case for four spots in melilite (II-5, III-13, III-15, and III-18), one spot (III-3) in fassaite, and one in anorthite (II-7). The cases of melilite II-5 and of anorthite II-7 are shown, together with that of an homogeneous melilite (III-8), as depth profiles (see electronic annex, EA1, EA2, and EA3, respectively). The most likely explanation for this observation is that the ion probe beam hit a mixture of different minerals, which were either exhausted or exposed during the sputtering. Second, contamination is apparent in melilite when looking, for instance, for correlations between Na_2O and Li or Be concentrations (Fig. 7). In Fig. 7, the "magmatic trend" points (black dots) tend to show an increase of [Be] and [Li] with increase of [Na_2O], which can be understood (see Section 4.1) as the result of crystal fractionation of a CAI melt produced from CAI precursors containing some low temperature alteration products. In contrast, the "non-magmatic trend" samples scatter over a very wide range of concentrations with half of them showing a correlation (curves in Fig. 7) pointing towards a composition that is Na_2O-free and Li–Be-rich. This correlation indicates mixing under the ion probe beam between unaltered melilite and another phase. The exact nature of this phase cannot be elucidated in the present study; however, we speculate that it could comprise small spinel grains altered at low temperature after the CAI last crystallized. Unaltered spinels are likely to be enriched in

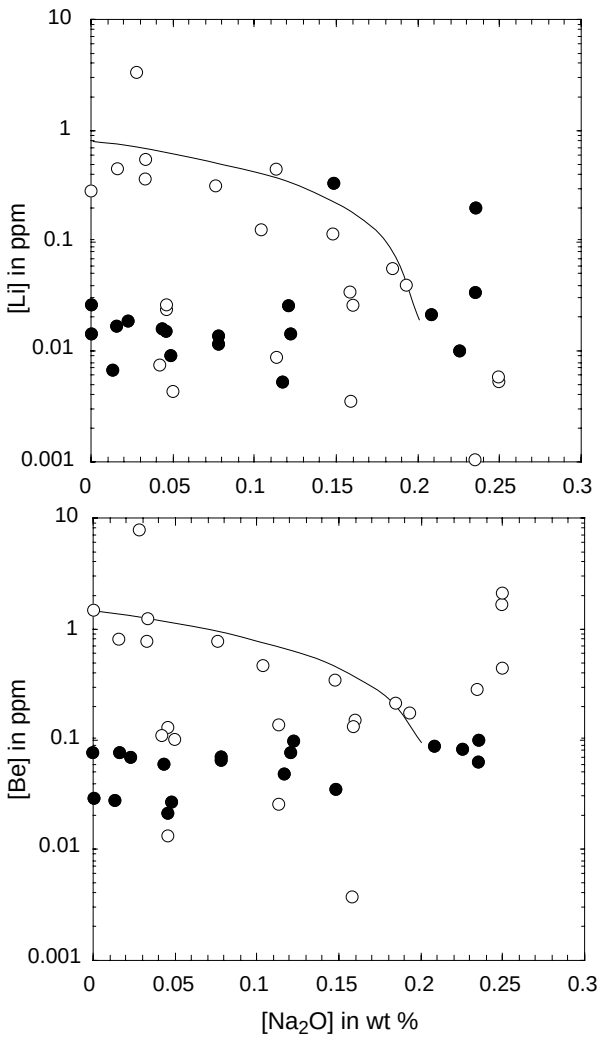

Fig. 7. Variations of Li and Be concentrations versus Na_2O concentrations in melilite (symbols as in Fig. 4). The increase of [Li] and [Be] with [Na_2O] observed for the black dots is compatible with magmatic fractionation. The two mixing lines (exponential in this semi-log diagram) indicate that half of the [Li] and [Be] variations observed in the open dots may be due to a mixing with Na-poor and Li–Be-rich phase (see text).

Be (which is refractory) and poor in Na (which is volatile). Re-melting and/or alteration were observed for spinel included in melilite in several CAIs (Burnett et al., 2004; Connolly et al., 2003), which affected their trace element contents (although Li was not measured in those studies). Other evidence suggests that alteration of spinels and spinel-rich areas may indeed cause enrichments in Li: (i) ion imaging of some spinel-rich areas in 3529-41 did show a strong Li signal coming from the spinels and (ii) TOF-SIMS studies imaged Li enrichments in Fe-rich phyllosilicates surrounding spinel in a CAI from the CM chondrite Cold Bokkeveld (Schirmeyer et al., 1997). Such an association has been interpreted as alteration products of melilite at the spinel–melilite interface (Greenwood et al., 1994).

4.2. B isotopic evidence for the incorporation of live ^{10}Be in Allende CAI 3529-41

The large B isotopic variations present in 3529-41 are positively correlated with the $^9Be/^{11}B$ ratios (Fig. 8). In contrast, the $^{10}B/^{11}B$ ratios are not well correlated with 1/[B] (Fig. 9) so that these B isotopic variations cannot be ascribed to simple mixing in the CAI between two components having inherited different B isotopic compositions. Additionally, the $^{10}B/^{11}B$ variations are far too large to be explained by mass-dependent fractionation processes, which also would not predict a correlation with $^9Be/^{11}B$. For these reasons, the correlation between $^{10}B/^{11}B$ and $^9Be/^{11}B$ is best explained as due to the in situ decay of radioactive ^{10}Be, in agreement with previous findings (McKeegan et al., 2000). The slope of this correlation yields a $^{10}Be/^9Be$ ratio at the time of closure of the

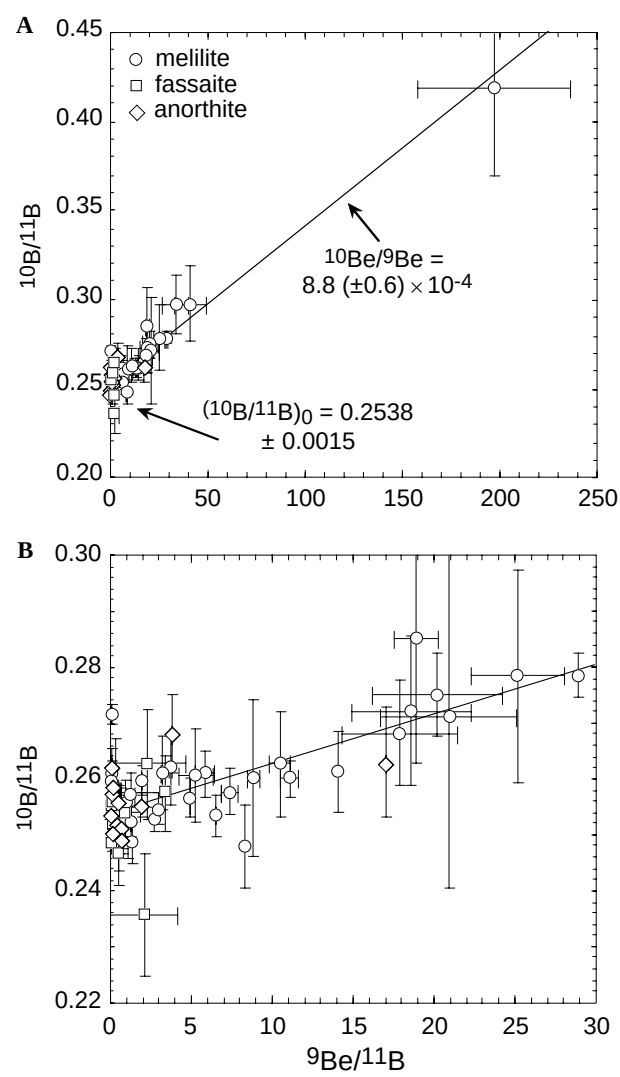

Fig. 8. Variations of $^{10}B/^{11}B$ ratios versus $^9Be/^{10}B$ ratios in (A) with blowup in (B). The positive correlation indicates that CAI incorporated short-lived ^{10}Be with a $^{10}Be/^9Be$ ratio of $8.8 \pm 0.6 \times 10^{-4}$ (see text for details). Note that very few perturbations of the $^{10}Be/^{10}B$ systems are observed.

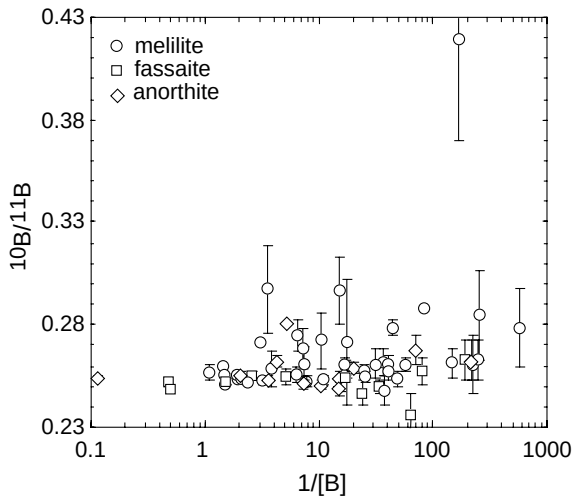

Fig. 9. Variations of ^{10}B/^{11}B ratios versus 1/[B]. Note that the B isotopic variations cannot be due to a mixing between two components having different isotopic compositions.

^{10}Be/B system $= 8.8 \pm 0.6 \times 10^{-4}$. This ratio is more precise but in perfect agreement with the ratio determined previously from a subset of 10 analytical spots in 3529-41 (^{10}Be/^{9}Be $= 9.5 \pm 1.9 \times 10^{-4}$, McKeegan et al., 2000). It corresponds to one of the highest ^{10}Be/^{9}Be ratios found in CAIs, which range from $1.1 \pm 0.5 \times 10^{-3}$ to $4.5 \pm 1.3 \times 10^{-4}$ (Chaussidon et al., 2001, 2003; MacPherson et al., 2003; Sugiura et al., 2001). The intercept of the ^{10}Be isochron yields an initial ^{10}B/^{11}B ratio $= 0.2538 \pm 0.0015$, corresponding to δ^{11}B $= -26 \pm 6$‰.

The ^{10}Be isochron is rather well defined with only two spots which plot significantly far from it (melilite II-5 and fassaite III-5). This simple behavior of the ^{10}Be/^{10}B system is striking in comparison to the ^{26}Al/^{26}Mg system because the ^{26}Al isochron (Podosek et al., 1991) shows significant perturbations in melilite (low ^{27}Al/^{24}Mg ratios) and also in a few anorthites (high ^{27}Al/^{24}Mg ratios). This apparent difference might be due to the fact that the precision on B isotopic ratios is worse than that on Mg isotopic ratios, thus possibly obscuring some disturbances of the Be–B system. However, stronger perturbations of the ^{26}Al/^{26}Mg system relative to the ^{10}Be/^{10}B system have been previously observed in other CAIs and were ascribed to the fact that B is likely to diffuse approximately two orders of magnitude more slowly than Mg (Sugiura et al., 2001). Another reason for the apparent robustness of ^{10}Be isochrons compared to ^{26}Al isochrons might be the difference in half-life between ^{10}Be ($T_{1/2} = 1.5$ My) and ^{26}Al ($T_{1/2} = 0.7$ My). For example, if the ^{26}Al/^{26}Mg system is reset 0.7 My after CAI crystallization, then the ^{26}Al/^{27}Al ratio will be lowered by a factor of 2 while the ^{10}Be/^{9}Be ratio would only be decreased by 30%. Thermal events, which might have occurred a few $\times 10^5$ years after CAI formation, could lead to a significant redistribution of radiogenic ^{26}Mg while having a relatively minor effect on ^{10}B.

The initial B isotopic ratio of 3529-41, δ^{11}B $= -26 \pm 6$‰, is significantly outside the range measured for bulk chondrites (from -10.5 ± 0.1‰ to $+19.2 \pm 0.2$‰; Zhai et al., 1996). Similar differences were previously noted for CAIs (Chaussidon et al., 2001) and a wide range of initial δ^{11}B values, from -60 to $+20$‰, have been derived from ^{10}Be isochrons in CAIs and in hibonite grains by several research groups (Chaussidon et al., 2001; MacPherson et al., 2003; Marhas and Goswami, 2003; Marhas et al., 2002; Sugiura et al., 2001). This range is likely to reflect the incorporation in CAI precursors of a fraction of B produced by spallation reactions together with ^{10}Be. Depending on the energy of the irradiation process, highly variable B isotopic ratios can theoretically be obtained: δ^{11}B ≈ -380‰ at GCR energies (0.5–1 GeV) and ≈ -130‰ $< \delta^{11}$B $< \approx +1700$‰ at lower (10–30 MeV) energies (Meneguzzi et al., 1971; Ramaty et al., 1996).

As discussed above (Section 4.1.1) and exemplified by the data in Fig. 6B, the large variability of [B] on small spatial scales in 3529-41 cannot be the result of magmatic crystal–melt fractionations, and thus a post-magmatic redistribution of B must have occurred in 3529-41. The timing of this redistribution is constrained by the observation that most of the points analyzed plot on a single ^{10}Be–^{10}B isochron, implying that this event must have occurred early in the post-magmatic history of 3529-41, i.e., before a significant fraction of ^{10}Be had decayed to ^{10}B. The rather low bulk B abundance in 3529-41 ($\approx$0.15 ppm) argues against the addition of much B from the matrix of Allende at a post-accretionary stage. This is corroborated by the inferred initial δ^{11}B of 3529-41, which is clearly lower than the bulk δ^{11}B of Allende (-0.56 ± 0.06‰, Zhai et al., 1996).

Interestingly, the two spots, which plot well off the ^{10}Be isochron in 3529-41, also show a very large range of B isotopic variations, from δ^{11}B $= -90 \pm 7$‰ for melilite spot II-5 to δ^{11}B $= +48 \pm 47$‰ for fassaite spot III-5 (Tables 4A and 4B). Melilite spot II-5(2) (see EA1) is also distinguished by having the lowest Li isotopic composition found in 3529-41 (or any CAI): ^{7}Li/^{6}Li $= 9.2 \pm 0.22$ (i.e., δ^{7}Li $= -235 \pm 24$‰). This ^{7}Li-poor isotopic composition is characteristic of Li produced by spallation reactions (^{7}Li/^{6}Li ranging from $\approx$1.5 to $\approx$6 depending on the energy, Ramaty et al., 1996). These observations suggest that the redistribution of B (and associated redistribution of Li and/or Be) occurred probably at a nebular stage when strong Li and B isotopic variations carried by irradiated gas and grains were still present in the nebula.

4.3. Li isotope anomalies in Allende CAI 3529-41: evidence for the incorporation of live ^{7}Be?

Points in melilite, fassaite, and pyroxene, which have [Li] and [Be] variations compatible with magmatic partitioning of these elements (Section 4.1.1), show large ^{7}Li/^{6}Li variations that are positively correlated with the ^{9}Be/^{6}Li ratios (Fig. 10). In contrast, points, which are characterized

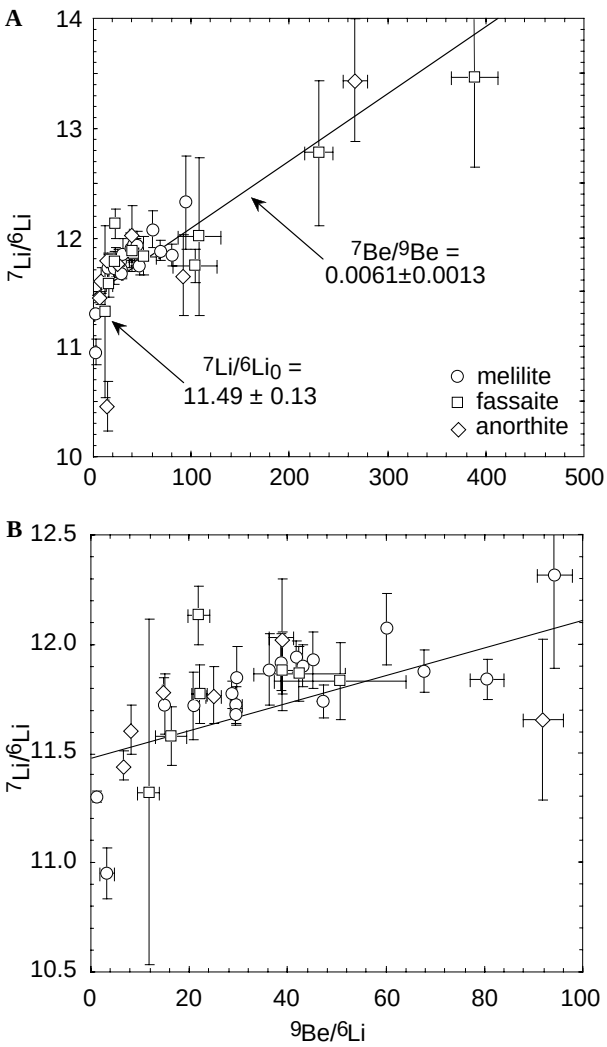

Fig. 10. Variations of ^{7}Li/^{6}Li ratios versus ^{9}Be/^{6}Li ratios, in (A) with blowup in (B), for the spots in 3529-41 which do not show obvious perturbations of their Li and Be distribution since magmatic partitioning during crystal fractionation of the CAI parent melt (see text). The positive correlation is consistent with the CAI having incorporated short-lived ^{7}Be at crystallization with a ^{7}Be/^{9}Be ratio of 0.0061 ± 0.0013 and that its ^{7}Li/^{6}Li ratio at that time was 11.49 ± 0.13.

by [Li] and [Be] variations showing post-magmatic perturbations, do not exhibit a correlation between ^{7}Li/^{6}Li and ^{9}Be/^{6}Li ratios (Fig. 12) and do not show any ^{7}Li/^{6}Li ratio higher than 12.

Two independent lines of argument strongly suggest that the correlation observed between ^{7}Li/^{6}Li and ^{9}Be/^{6}Li ratios (Fig. 10) is due to the in situ decay of radioactive ^{7}Be. First, because of the very high diffusivity of Li in melts, it is not conceivable that the ^{7}Li/^{6}Li variations observed could be inherited from the CAI precursors or from Li isotopic heterogeneities present at a magmatic stage. The Li diffusivity is $\approx 6 \times 10^{-5}$ cm^2/s at 1350 °C in basaltic melts (Richter et al., 2003) which is two orders of magnitude higher than any other species except molecular water. With such a fast diffusivity, Li isotopic variations, if present among CAI precursors or in the CAI melt, would be erased in ≈ 5 h at the centimeter scale. Thus, the only way to produce ^{7}Li excesses after crystallization of the CAI, without modifying the [Li] and [Be] inherited from magmatic crystal fractionation and preserving a correlation with the ^{9}Be/^{6}Li ratio, would seem to be the in situ decay of ^{7}Be.

The second line of reasoning pointing toward the former presence of live ^{7}Be follows from the observation that the measured ^{7}Li/^{6}Li variations cannot be explained by a post-magmatic mixing process between two Li components because there is no plausible candidate for the high ^{7}Li/^{6}Li component. Of critical importance is the fact that the positive correlation between ^{7}Li/^{6}Li and ^{9}Be/^{6}Li ratios extends to ^{7}Li/^{6}Li ratios significantly higher than 12 (up to 13.5). However, there is no Li known in meteorites with ^{7}Li/^{6}Li ≈ 13.5 (or greater), which could explain the presence of such a component in the CAI. Bulk chondritic Li has a ^{7}Li/^{6}Li $= 12.02$ (James and Palmer, 2000; McDonough et al., 2003) and spallogenic Li is characterized by ^{7}Li/^{6}Li $<< 12$ (Meneguzzi et al., 1971; Ramaty et al., 1996; Read and Viola, 1984).

It is important to stress here that these high ^{7}Li/^{6}Li ratios are not due to an over-correction for spallogenic Li produced during the exposure of the Allende meteoroid to GCR (see Section 3.2.2). Such an over-correction would result in ^{7}Li/^{6}Li being higher than 12 for any spot having very low [Li] and this is obviously not the case. In fact, the spots which do not show a magmatic partitioning of Li and Be, and which have [Li] < 0.001 ppm (e.g., spots III-3(1), II-2, II-3, and II-10-2 in Table 4B), all have ^{7}Li/^{6}Li < 12 (see Fig. 12 or points with high ^{9}Be/^{6}Li in Fig. 11). Finally, it should also be noted that because Li is, on average, more incompatible than Be during crystal fractionation, there is a general tendency for ^{9}Be/^{6}Li ratios to increase with decreasing [Li] for the spots showing a

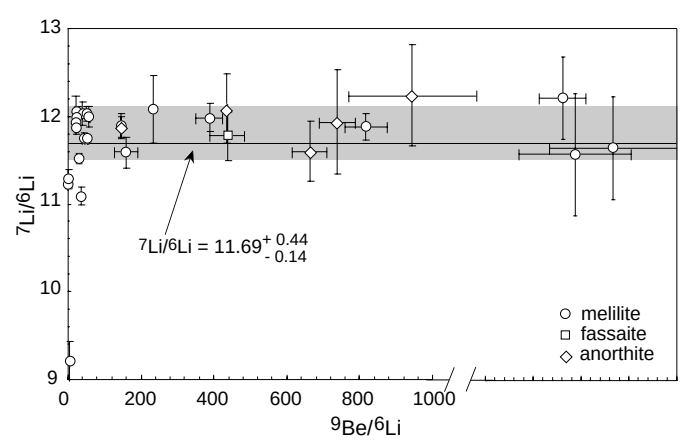

Fig. 11. Variations of ^{7}Li/^{6}Li ratios versus ^{9}Be/^{6}Li ratios in 3529-41 in spots where the original magmatic Li and Be distributions were perturbed by post-magmatic events. Note that there is no correlation between ^{7}Li/^{6}Li and ^{9}Be/^{6}Li, and that no ^{7}Li/^{6}Li higher than ≈ 12 is observed. Note that the average ^{7}Li/^{6}Li ratio of these spots is equal to 11.72 ± 0.56, i.e., the value which can be calculated by mass balance (gray field) for Li isotopic homogenization after the decay of ^{7}Be.

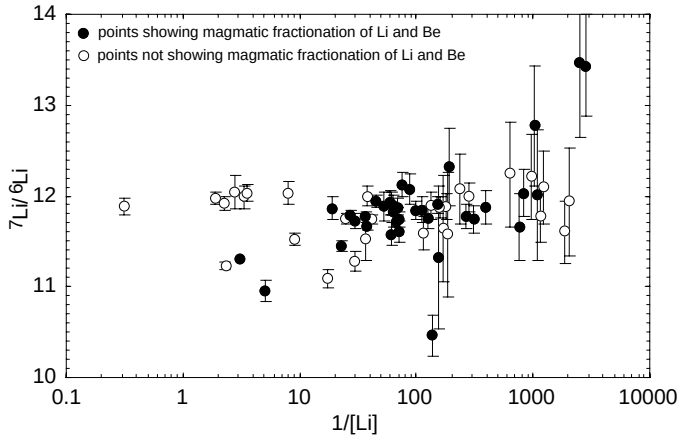

Fig. 12. Variations of ^{7}Li/^{6}Li ratios versus 1/[Li] in 3529-41 (different mineral phases are not indicated by specific symbols). No clear mixing trend is observed for 3529-41. Note, however, that because of the partitioning behavior of Li and Be during crystal fractionation, the ^{9}Be/^{6}Li ratios are broadly correlated with 1/[Li] (see text for details) so that the correlation observed in Fig. 10 implies a rough correlation for the black spots in this figure.

magmatic Li and Be distribution. Thus, an argument postulating a correlation between ^{7}Li/^{6}Li ratios and 1/[Li] cannot be taken as an indication of mixing between two components because if ^{7}Li/^{6}Li ratios are positively correlated with ^{9}Be/^{6}Li ratios they will necessarily be broadly correlated with 1/[Li]. Note, however (Fig. 12), that this correlation is not so clear and that it does not exist in 3529-41 as a whole, ruling out a simple addition of "exotic" Li to the CAI to explain the Li isotopic variations.

Considering all the petrographic and isotopic evidence, the most likely interpretation of the positive correlation between ^{7}Li/^{6}Li and ^{9}Be/^{6}Li ratios (Fig. 10) is the in situ decay of radioactive ^{7}Be. A best fit line calculated through all the points showing Li–Be magmatic partitioning (Fig. 10) gives a ^{7}Be/^{9}Be slope of 0.0061 ± 0.0013 and an initial ^{7}Li/^{6}Li ratio at the time of crystallization of 11.49 ± 0.13. The slope of ^{7}Be isochron is strongly constrained by the few points having very high ^{9}Be/^{6}Li ratios but this slope seems rather robust. In fact, the best fit line calculated from the melilites only (which have lower ^{9}Be/^{6}Li ratios and no Li isotopic correction in excess of a few ‰ due to GCR contribution) gives a slope of 0.0081 ± 0.0031 and an initial of 11.50 ± 0.15, in good agreement within errors with the regression line calculated from all the points.

The average ^{7}Li/^{6}Li ratio of those points, which do not show any correlation between the ^{7}Li/^{6}Li ratios and the ^{9}Be/^{6}Li ratios, is 11.72 ± 0.56. As previously discussed (Section 4.1), a post-magmatic redistribution of Li and Be in the CAI is likely the cause of the non-magmatic distribution of Li and Be observed for a number of analytical spots in 3529-41. Li isotopic mass balance is in agreement with such a scenario: taking an average ^{9}Be/^{6}Li ratio of $33.5^{+71.8}_{-22.8}$ for 3529-41 (logarithmic mean of all the points) and a ^{7}Be/^{9}Be of 0.0061, a mean ^{7}Li/^{6}Li of $11.69^{+0.44}_{-0.14}$ can be calculated for phases in the CAI which would have been homogenized isotopically for Li after ^{7}Be was extinct. This ^{7}Li/^{6}Li ratio of 11.69 is identical to the mean of the points having a non-magmatic distribution of Li and Be (Fig. 11). The first stage of this isotopic homogenization may be seen in melilite spots III-1-3, III-9, and III-15-1 which are off but not far from the "magmatic trend" of Fig. 4 and which plot below the ^{7}Be isochron. This may occur by diffusion during cooling and re-heating events either in the nebula or in the planetesimal where the CAI was incorporated. The timescales for cooling during metamorphism in a planetesimal are much longer than those for cooling in the nebula. Experimental studies of the diffusion of Mg in anorthite (LaTourette and Wasserburg, 1998) and of K in melilite (Ito and Ganguly, 2004) have shown that ^{26}Mg and ^{41}K excesses due to the in situ decay of ^{26}Al and ^{41}Ca can be preserved in CAIs for specific sizes of the planetesimal and "depth" of the CAI in the planetesimal. Experimental data for Li diffusion in melilite are lacking so that the degree of preservation of Li isotopic variations during the metamorphic history of planetesimals cannot be predicted at present.

Finally, it can be noted that, similar to the ^{10}Be isochron, a few points plot either significantly off the ^{7}Be isochron (e.g., melilite spot III-18 with ^{7}Li/^{6}Li $= 10.95 \pm 0.12$ in Fig. 10) or very far from the mean ^{7}Li/^{6}Li ratio of the "bulk CAI" (e.g., melilite II-5 with ^{7}Li/^{6}Li $= 9.2 \pm 0.22$ in Fig. 11). As discussed for B isotopes in the previous section, these points likely correspond to spots where the ion probe beam sampled alteration products rich in spallogenic Li (and B). These alteration products were introduced in the CAI probably at a nebular stage before the CAI was accreted to the meteorite parent body with matrix material having a ^{7}Li/^{6}Li ratio $\approx$12.

In summary, the variation of Li isotopic compositions in 3529-41 is in agreement with the following simplified scenario: (i) 3529-41 was assembled from a variety of precursors, Be being possibly contained in the more refractory ones but Li being mostly contained in lower temperature phases, which contained radioactive ^{7}Be and ^{10}Be, in addition to other spallation nuclides, (ii) during the last melting event Li and Be were homogenized isotopically to ^{7}Be/^{9}Be $= 0.0061 \pm 0.013$, ^{10}Be/^{9}Be $= 8.8 \pm 0.6 \times 10^{-4}$, and ^{7}Li/^{6}Li $= 11.49 \pm 0.13$ and minerals crystallized with magmatic partitioning of Li–Be–B and with incorporation of live ^{7}Be and ^{10}Be into their lattices (iii) at a later time, at least ~500 days later (when ^{7}Be was extinct), some of the Li distributions were perturbed in the CAI by a secondary process such as re-heating and, in those places, Li isotopic compositions were locally homogenized by diffusion to reach a ^{7}Li/^{6}Li of $\approx$11.69, (iv) at this stage or possibly later (but still in a nebular environment) some spallogenic-rich Li (together with spallogenic-rich B) was added to the CAI, (v) after final cooling, isotopic closure was attained for B and Mg and radiogenic ^{10}B and ^{26}Mg accumulated from the decay of ^{10}Be and ^{26}Al, respectively.

4.4. Implications for irradiation processes in the early solar system

4.4.1. Origin of the low $^7Li/^6Li$ initial ratio of CAIs

The initial $^7Li/^6Li$ ratio in 3529-41 (11.49 ± 0.13) is significantly lower (by $\approx 44‰$) than the bulk chondritic (or bulk terrestrial) ratio of 12.02. Such a difference cannot be the result of an isotopic fractionation which would be associated with the formation of CAIs. In fact, Li isotopic fractionations between melt and crystal are negligible at high temperatures (Tomascak et al., 1999). The only fractionation process, which could lead to large shifts in the Li isotopic composition of a CAI melt, is evaporation. However, in case of an evaporative loss of Li, the Li remaining in the CAI can be expected to be enriched in the heavy isotope, ^7Li (Davis et al., 1990), contrary to what is observed in 3529-41. Thus, the low $^7Li/^6Li$ initial ratio of CAIs most likely implies that CAI precursors were depleted in ^7Li relative to bulk solar system represented by chondrites and by the terrestrial mantle.

The simplest way to understand this difference is to appeal to the presence of Li in CAI precursors with a spallogenic component exceeding that which characterizes average solar system matter. Assuming relative production ratios for $^6Li/^9Be$ and $^7Li/^6Li$ of ~ 40 and ~ 2.5, respectively, at 10 MeV (Ramaty et al., 1996), such as would be characteristic for irradiation around the early Sun, and taking a bulk solar system ratio for $Li/Be = 77$ (Anders and Grevesse, 1989), we calculate that to produce $\sim 0.1\%$ of new spallogenic Be (corresponding to $^{10}Be/^9Be = 10^{-3}$), approximately 2% of the Li should be also produced by spallation. If added to chondritic Li, such a component would yield $^7Li/^6Li = 11.42$, which is in very good agreement with the initial $^7Li/^6Li$ ratio inferred for 3529-41 (11.49 ± 0.13). Thus, the initial $^7Li/^6Li$ and $^{10}Be/^9Be$ ratios of 3529-41 are consistent with a common production during low energy irradiation events. In contrast, this spallogenic component, which seems to be present in most CAIs, is apparently largely absent from bulk chondrites as indicated by their high $^7Li/^6Li$ ratios. This observation is important because it indicates that if irradiation processes were ubiquitous in the CAI-forming regions, possibly around the early Sun, then only a small fraction of the material in chondrites was exposed to this environment.

4.4.2. Production of ^7Be, ^{10}Be, and other extinct radionuclides during early solar system irradiation

Given that the Li–Be–B isotopic signatures of CAIs are best understood as recording irradiation of their precursors by energetic particles, the question arises as to where (and when) this irradiation took place. Following the discovery of the former presence of ^{10}Be in an Allende CAI, we argued that the most likely source involved irradiation within the solar nebula (McKeegan et al., 2000). The status of ^{10}Be as a 'smoking gun' for irradiation by solar energetic particles (Gounelle et al., 2001) was impugned by the possibility that much of the ^{10}Be was inherited from the molecular cloud phase immediately prior to isolation and collapse of the solar accretion disk (Desch et al., 2004). Although other evidence characteristic of irradiation processes, such as apparent spallogenic Li in CAI precursors that is isotopically different than bulk chondrite, is difficult to explain in terms of large-scale processes such as GCR trapping, the relatively long time interval given by the 1.5 Ma half-life of ^{10}Be permits significant ambiguity regarding the locale where it was synthesized.

On the other hand, the very short half-life of ^7Be of 53 days dictates that this nuclide must have been produced essentially contemporaneously with the formation of CAI 3529-41 and that it cannot have been inherited from the pre-solar cloud. Because ^7Be can only be produced by spallation reactions, a source of accelerated particles is required for its nucleosynthesis. Such a source is most likely the Sun in its pre-T-Tauri or T-Tauri phase, as indicated by observations of young stellar objects which show strong X-ray luminosities of the order of 4.5×10^{29} erg s^{-1}, with frequent X-ray flares enhancement by a factor of $\approx 10^4$, implying associated intense fluxes of accelerated particles (Feigelson and Montmerle, 1999; Feigelson et al., 2002). Models, such as the x-wind scenario of Shu and colleagues (Shu et al., 1996, 1997, 2001), provide a physical framework in which refractory dust grains and gas are irradiated by solar cosmic rays at very close heliocentric distances of ≈ 0.06 AU. In this model, while most of the matter accreting to the Sun is driven through funnel flows, a portion of it can migrate inward of the corotation terminus of the accretion disk into a relatively gas-free region characterized by magnetic reconnection flares. Because there is essentially no shielding in this "reconnection ring," irradiation by energetic protons and alpha particles is efficient and intense. Due to proximity to the protoSun, thermal processing is severe. A fraction of the grains, which either survived evaporation in the reconnection ring or recondensed in this region, can then be extracted by fluctuations of the x-point and be launched by a disk wind (the x-wind) to heliocentric distances of several AU. The models infer that these stochastic processes occur on characteristic timescales of approximately 1–10 years which then represents the time available for irradiation of dust grains and gas–solid condensates that may form precursors of CAIs (Gounelle et al., 2001).

Calculations have been developed in the context of the x-wind model to determine the possible production rates of extinct radionuclides observed in CAIs (Gounelle et al., 2001; Gounelle et al., submitted; Lee et al., 1998; Leya et al., 2003). It is beyond the scope of the present work to critically appraise these calculations; however, it is a matter of fact that all the models successfully reproduce the $^{10}Be/^9Be$ ratio observed in 3529-41 and differ in their predictions for the $^7Be/^9Be$ ratio in 3529-41 which is reproduced by Gounelle et al. (2004) and is slightly too high compared to calculations by Leya et al. (2003). Because of saturation effects, the abundance of ^7Be reflects production over at most 1 year irradiation while the

amount of ^{10}Be can correspond to an accumulation over a much longer period. Thus, it is expected that some variations of these ratios should be observed as a function of irradiation parameters (e.g., the chemistry of the irradiated targets or of the energy spectrum and composition of the energetic particles) as well as irradiation duration. In conjunction with the petrographic complexities in preserving remnants of a ^{7}Be–Li isochron in a given CAI, it seems that it will be unlikely for further investigations to find a characteristic or 'canonical' value for the ratio of ^{7}Be/^{9}Be relative to ^{10}Be/^{9}Be. Nevertheless, the mere presence of ^{7}Be in 3529-41, whatever its abundance, indicates a strong irradiation of its precursors within a short time of its formation. It also strongly suggests that the ^{10}Be, which is found nearly ubiquitously in CAIs, is mostly made in the same process. This process is most likely irradiation of the CAIs or of their precursors in the reconnection ring near the early Sun. The calculations also show that, with some uncertainty, the production of other short-lived radionuclides (^{26}Al, ^{41}Ca, and ^{53}Mn) is possible at the levels observed in CAIs but that this requires layered compositions of the targets and special spectra for the accelerated particles. However, other models (Goswami et al., 2001; Marhas and Goswami, 2003; Marhas et al., 2002) disagree on this point (see Chaussidon and Gounelle, in press, for a review of these models, of their predictions, and of their uncertainties). Finally, it must be stressed that the difference in Li isotopic ratios between bulk chondrites and bulk CAI (or CAI initial) suggests that only a small fraction of the matter constituting the chondrites was irradiated. Nevertheless, the presence of ^{7}Be in 3529-41 demonstrates that irradiation processes were present in the early solar system and must be taken into account to understand the formation and the evolution of the earliest solids.

5. Conclusions

Large variations in the concentrations and isotopic compositions of lithium and boron are found in Allende CAI 3529-41. Isotopic compositions, corrected for recent exposure to GCR, range from ^{7}Li/^{6}Li $= 9.2 \pm 0.22$ to 13.44 ± 0.56 and ^{10}B/^{11}B $= 0.2468 \pm 0.0057$ to 0.4189 ± 0.0493. The ^{10}B/^{11}B ratios are positively correlated with ^{9}Be/^{11}B in a manner indicating the in situ decay of short-lived ^{10}Be (half-life = 1.5 Ma) with a ^{10}Be/^{9}Be ratio at the time of formation of the CAI of $8.8 \pm 0.6 \times 10^{-4}$. Disturbances in the Be–B system are minimal, but the distribution of B in the CAI indicates some post-magmatic introduction of boron into the CAI. This redistribution of boron is qualitatively commensurate with evidence for nebular alteration based on distributions of other moderately volatile elements, including Na and Mg, and has implications for discriminating primary Li isotopic signatures from those introduced by secondary processes.

Based on experimental and inferred partition coefficients, a subset of points analyzed in 3529-41 have Li and Be concentration distributions that may be consistent with closed-system crystallization of the CAI melt. In these spots of melilite, anorthite, and fassaite, many of which also contain included spinel, ^{7}Li/^{6}Li isotopic variations (corrected for GCR exposure) are positively correlated with ^{9}Be/^{6}Li suggesting the in situ decay of now-extinct ^{7}Be. The model isochron implies that at the time of its formation, the CAI melt had a ^{7}Be/^{9}Be ratio of 0.0061 ± 0.0013 and a ^{7}Li/^{6}Li ratio of 11.49 ± 0.13. The 56% of the spots in melilite, 38% in anorthite, and 8% in fassaite, which show evidence for post-magmatic redistribution of Li and/or Be (according to our criteria), have relatively constant ^{7}Li/^{6}Li, averaging 11.72 ± 0.56, which is consistent with mass balance calculations for Li isotopic homogenization in the CAI after the decay of ^{7}Be. Because of its very short half-life, the ^{7}Be must have been produced contemporaneously with the formation of the CAI by irradiation processes within the solar accretion disk during the early stages of its evolution. These processes are capable of producing ^{10}Be in the abundances observed in many CAIs and also a significant fraction of other short-lived radionuclides observed in early solar system materials.

Acknowledgements

We thank Guy Libourel, Matthieu Gounelle, Jean Duprat, and Ingo Leya for stimulating discussions and thoughtful advice, and Shogo Tachibana and two anonymous reviewers for their comments and suggestions. Allende CAI 3529-41 was kindly made available by Glenn MacPherson, curator of meteorites at the Smithsonian Institution. This work was supported by PNP-INSU grants and Région Lorraine grants to Marc Chaussidon; Kevin McKeegan gratefully acknowledges support from the NASA Cosmochemistry Program. This is CRPG contribution number 1777.

Associate Editor: Alexander N. Krot

Appendix A. Supplementary data

Supplementary data associated with this article can be found, in the online version, at doi:10.1016/j.gca.2005.08.016.

References

Anders, E., Grevesse, N., 1989. Abundance of the elements: meteoritic and solar. *Geochim. Cosmochim. Acta* **53**, 197–214.

Beck, P., Barrat, J.A., Chaussidon, M., Gillet, P., Bohn, M., 2004. Li isotopic variations in single pyroxenes from the Northwest Africa 480 shergottite (NWA 480): a record of degassing of Martian magmas? *Geochim. Cosmochim. Acta* **68**, 2925–2933.

Beckett, J.R., Stolper, E., 2000. The partitioning of Na between melilite and liquid: Part I. The role of crystal chemistry and liquid composition. *Geochim. Cosmochim. Acta* **64**, 2509–2517.

Beckett, J.R., Simon, S.B., Stolper, E., 2000. The partitioning of Na between melilite and liquid: Part II. Application to type B inclusions

from carbonaceous chondrites. *Geochim. Cosmochim. Acta* **64**, 2519–2534.

Beckett, J.R., Spivack, A.J., Hutcheon, I.D., Wasserburg, G.J., Stolper, E.M., 1990. Crystal chemical effects on the partitioning of trace elements between mineral and melt: an experimental study of melilite with application to refractory inclusions from carbonaceous chondrites. *Geochim. Cosmochim. Acta* **54**, 1755–1774.

Bourot-Denise, M., Pellas, P., 1982. Cosmic ray track densities and ^{60}Co activities as depth monitors in Allende meteoroid. *Meteoritics* **17**, 186.

Brearley, A.J., Jones, R.H., 1998. Chondritic meteorites. In: Papike, J.J. (Ed.), *Reviews in Mineralogy*, vol. 36. Mineralogical Society of America, Washington, DC, USA, pp. 3-1–3-198.

Brenan, J.M., Neroda, E., Lundstrom, C.C., Shaw, H.F., Ryerson, F.J., Phinney, D.L., 1998. Behavior of boron, beryllium and lithium during melting and crystallization: constraints from mineral–melt partitioning experiments. *Geochim. Cosmochim. Acta* **62**, 2129–2141.

Burnett, D.S., Paque, J.M., Beckett, J.R., 2004. Zoning patterns in spinel from type B Ca–Al-rich inclusions: constraints on sub-solidus thermal history (abstract). *Lunar Planet. Sci.* **XXXV**, 1253.

Cassé, M., Lehoucq, R., Vangioni-Flam, 1995. Production and evolution of light elements in active star forming regions. *Nature* **373**, 318–319.

Chaussidon, M., Gounelle, M., in press. Irradiation processes in the early solar system. In: Lauretta, D.S., McSween, H.Y. (Eds.), *Meteorites and Early Solar System II*. University of Arizona Press.

Chaussidon, M., Robert, F., 1998. ^{7}Li/^{6}Li and ^{11}B/^{10}B variations in chondrules from the Semarkona unequilibrated chondrite. *Earth Planet. Sci. Lett.* **164**, 577–589.

Chaussidon, M., Robert, F., McKeegan, K.D., 2001. Lithium and boron isotopic compositions of refractory inclusions from primitive chondrites: a record of irradiation in the early solar system (abstract). *Lunar Planet. Sci.* **32**, 1862.

Chaussidon, M., Robert, F., McKeegan, K.D., 2002. Incorporation of short-lived ^{7}Be in one CAI from the Allende meteorite (abstract). *Lunar Planet. Sci.* **33**, 1563.

Chaussidon, M., Robert, F., Mangin, D., Hanon, P., Rose, E., 1997. Analytical procedures for the measurement of boron isotope compositions by ion microprobe in meteorites and mantle rocks. *Geostand. Newsl.* **21**, 7–17.

Chaussidon, M., Robert, F., Russel, S.S., Gounelle, M., Ash, R.D., 2003. Variations of apparent ^{10}Be/^{9}Be ratios in Leoville MRS-06 type B1 CAI: constraints on the origin of ^{10}Be and ^{26}Al (abstract). *Lunar Planet. Sci.* **34**, 1347.

Connolly, H.C., Burnett, D.S., McKeegan, K.D., 2003. The petrogenesis of type B1 Ca–Al rich inclusions: the spinel perspective. *Meteorit. Planet. Sci.* **38**, 197–224.

Davis, A.M., Hashimoto, A., Clayton, R.N., Mayeda, T.K., 1990. Isotope mass fractionation during evaporation of Mg_2SiO_4. *Nature* **347**, 655–658.

Decitre, S., Deloule, E., Reisberg, L., James, R., Agrinier, P., Mevel, C., 2002. Behaviour of Li and its isotopes during serpentinization of oceanic peridotites. *Geochem. Geophys. Geosyst.*, 3. doi:10.1029/2001GC000178.

Desch, S.J., Connolly, H.C., Srinivasan, G., 2004. An interstellar origin for the beryllium-10 in calcium-rich, aluminum-rich inclusions. *Astrophys. J.* **602**, 528–542.

Feigelson, E.D., Montmerle, T., 1999. High energy processes in young stellar objects. *Annu. Rev. Astron. Astrophys.* **37**, 363–408.

Feigelson, E.D., Garmire, G.P., Pravdo, S.H., 2002. Magnetic flaring in the pre-main-sequence sun and implications for the early solar system. *Astrophys. J.* **572**, 335–349.

Fireman, E.L., Goebel, R., 1970. Argon-37 and argon-39 in recently fallen meteorites and cosmic ray variations. *J. Geophys. Res.* **75**, 2115–2124.

Goswami, J.N., Marhas, K.K., Sahijpal, S., 2001. Did solar energetic particles produce the short-lived radionuclides present in the early solar system? *Astrophys. J.* **549**, 1151–1159.

Gounelle, M., Shu, F.H., Shang, H., Glassgold, A.E., Rehm, E.K., Lee, T., 2004. The origin of short-lived radionuclides and early Solar System irradiation (abstract). *Lunar Planet. Sci.* **35**, 1829.

Gounelle, M., Shu, F.H., Shang, H., Glassgold, A.E., Rehm, K.R., Lee, T., 2001. Extinct radioactivities and protostellar cosmic rays: self shielding and light elements. *Astrophys. J.* **548**, 1051–1070.

Govindaraju, K., 1989. Compilation of working values and sample description for 272 geostandards. *Geostand. Newsl.* **13**, 1–113.

Greenwood, R.C., Lee, M.R., Hutchison, R., Barber, D.J., 1994. Formation and alteration of CAIs in Cold Bokkeveld (CM2). *Geochim. Cosmochim. Acta* **58**, 1913–1935.

Grossman, L., 1975. Petrography and mineral chemistry of Ca-rich-inclusions in the Allende meteorite. *Geochim. Cosmochim. Acta* **39**, 433–454.

Herd, C.D.K., Treiman, A.H., McKay, G.A., Shearer, C.K., 2004. The behavior of Li and B during planetary basalt crystallization. *Am. Mineral.* **89**, 832–840.

Hinton, R.W., 1990. Ion microprobe trace-element analysis of silicates: measurement of multi-element glasses. *Chem. Geol.* **83**, 11–25.

Ito, M., Ganguly, J., 2004. Potassium diffusion in melilite: experimental studies and constraints on the thermal history and size of planetesimals hosting CAIs. *Meteorit. Planet. Sci.* **39**, 1911–1919.

James, R.H., Palmer, M.R., 2000. The lithium isotope composition of international rock standards. *Chem. Geol.* **166**, 319–326.

LaTourette, L., Wasserburg, G.J., 1998. Mg diffusion in anorthite: implications for the formation of early solar system planetesimals. *Earth Planet. Sci. Lett.* **158**, 91–108.

Lauretta, D.S., Lodders, K., 1997. The cosmochemical behavior of beryllium and boron. *Earth Planet. Sci. Lett.* **146**, 315–327.

Lee, T., Shu, F.H., Shang, H., Glassgold, A.E., Rhem, K.E., 1998. Protostellar cosmic rays and extinct radioactivities in meteorites. *Astrophys. J.* **506**, 898–912.

Leya, I., Lange, H.-J., Neumann, S., Wieler, R., Michel, R., 2000a. The production of cosmogenic nuclides in stony meteoroids by galactic cosmic-ray particles. *Meteorit. Planet. Sci.* **35**, 259–286.

Leya, I., Lange, H.-J., et al., 2000b. Simulation of the interaction of galactic cosmic rays protons with meteoroids: on the production of radionuclides in thick gabbro and iron targets irradiated isotropically with 1.6 GeV protons. *Meteorit. Planet. Sci.* **35**, 287–316.

Leya, I., Halliday, A.N., Wieler, R., 2003. The predictable collateral consequences of nucleosynthesis by spallation reactions in the early Solar System. *Astrophys. J.* **594**, 605–616.

MacPherson, G.J., Huss, G.R., Davis, A.M., 2003. Extinct ^{10}Be in type A calcium–aluminum-rich inclusions from CV chondrites. *Geochim. Cosmochim. Acta* **67**, 3165–3179.

MacPherson, G.J., Wark, D.A., Armstrong, J.T., 1988. Primitive material surviving in chondrites: refractory inclusions. In: Kerridge, J.F., Matthew, M.S. (Eds.), *Meteorites and the Early Solar System*. University of Arizona Press, pp. 746–807.

Marhas, K.K., Goswami, J.N., 2003. Be–B isotope systematics in CV and CM hibonites: implications for solar energetic particle production of short-lived nuclides in early solar system (abstract). *Lunar Planet. Sci.* **34**, 1303.

Marhas, K.K., Goswami, J.N., Davis, A.M., 2002. Short-lived nuclides in hibonite grains from Murchison: evidence for solar system evolution. *Science* **298**, 2182–2185.

McDonough, W.F., Teng, F.Z., Tomascak, P.B., Ash, R.D., Grossman, J.N., Rudnick, R.L., 2003. Lithium isotopic composition of chondritic meteorites (abstract). *Lunar Planet. Sci.* **34**, 1931.

McKeegan, K.D., Chaussidon, M., Robert, F., 2000. Incorporation of short-lived ^{10}Be in a calcium–aluminum-rich inclusion from the Allende meteorite. *Science* **289**, 1334–1337.

Meneguzzi, M., Audouze, J., Reeves, H., 1971. The production of the elements Li, Be, B by galactic cosmic rays in space and its relation with stellar observations. *Astron. Astrophys.* **15**, 337–359.

Michel, R., Leya, I., Borges, L., 1996. Production of cosmogenic nuclides in meteoroids: accelerator experiments and model calculation to decipher the cosmic ray record in extraterrestrial matter. *Nucl. Instrum. Methods Res. Phys. B* **113**, 433–444.

Michel, R., Peiffer, F., Theis, S., Begemann, F., Weber, H., Signer, P., Wieler, R., Cloth, P., Dragovitsch, P., Filges, D., Englert, P., 1989.

Production of stable and radioactive nuclides in thick stony targets ($R = 15$ and 25 cm) isotropically irradiated with 600 MeV protons and simulation of the production of cosmogenic nuclides in small meteorites. *Nucl. Instrum. Methods Phys. Res. B* **42**, 76–100.

Paque, J.M., Burnett, D.S., Chaussidon, M., 2003. UNSM 3515: an Allende CAI with Li isotopic variations (abstract). *Lunar Planet. Sci.* **34**, 1401.

Phinney, D., Whitehead, B., Anderson, D., 1979. Li, Be, and B in minerals of a refractory-rich Allende inclusion. In: *Proceedings of the Lunar Planetary Science Conference 10th*, pp. 885–905.

Podosek, F.A., Zinner, E.K., MacPherson, G.J., Lundberg, L.L., Brannon, J.C., Fahey, A.J., 1991. Correlated study of initial ^{87}Sr/^{86}Sr and Al–Mg systematics and petrologic properties in a suite of refractory inclusions from the Allende meteorite. *Geochim. Cosmochim. Acta* **55**, 1083–1110.

Ramaty, R., Kozlovski, B., Lingenfelter, R.E., 1996. Light isotopes, extinct radioisotopes and gamma-ray lines from low-energy cosmic rays interactions. *Astrophys. J.* **456**, 525–540.

Read, S.M., Viola, V.E., 1984. Excitation function for A > 6 fragments formed in ^{1}H and ^{4}He-induced reactions on light nuclei. *At. Data Nucl. Data Tables* **31**, 359–385.

Reeves, H., 1994. On the origin of the light elements ($Z < 6$). *Rev. Mod. Phys.* **66**, 193–216.

Richter, F.M., Davis, A.M., DePaolo, D.J., Watson, E.B., 2003. Isotope fractionation by chemical diffusion between molten basalt and rhyolite. *Geochim. Cosmochim. Acta* **67**, 3905–3923.

Robert, F., Chaussidon, M., 2003. Boron and lithium isotopic composition in chondrules from the Mokoia meteorite (abstract). *Lunar Planet. Sci.* **34**, 1344.

Ryan, J.G., Langmuir, C.H., 1987. The systematics of lithium abundances in young volcanic rocks. *Geochim. Cosmochim. Acta* **51**, 1727–1741.

Ryan, J.G., Langmuir, C.H., 1988. Beryllium systematics in young volcanic rocks: implications for ^{10}Be. *Geochim. Cosmochim. Acta* **52**, 237–244.

Scherer, P., Schultz, L., 2000. Noble gas record, collisional history, and pairing of CV, CO, CK and other carbonaceous chondrites. *Meteorit. Planet. Sci.* **35**, 145–153.

Schirmeyer, S., Hoppe, P., Stephan, T., Bischoff, A., Jessberger, E.K., 1997. A lithium-bearing Ca,Al-rich inclusion from the CM-chondrite Cold Bokkeveld studied by TOF-SIMS and conventional SIMS (abstract). *Lunar Planet. Sci.* **28**, 1377.

Shu, F.H., Shang, H., Lee, T., 1996. Towards an astrophysical theory of chondrites. *Science* **271**, 1545–1552.

Shu, F.H., Najita, J., Ostriker, E., Wilkin, F., Rude, S., Lizano, S., 1994. Magnetocentrifugally driven flows from young stars and disks. I: a generalized model. *Astrophys. J.* **429**, 781–796.

Shu, F.H., Shang, H., Glassgold, A.E., Lee, T., 1997. X-rays and fluctuating X-winds from protostars. *Science* **277**, 1475–1479.

Shu, F.H., Shang, S., Gounelle, M., Glassgold, A.E., Lee, T., 2001. The origin of chondrules and refractory inclusions in chondritic meteorites. *Astrophys. J.* **548**, 1029–1050.

Simon, S.B., Grossman, L., Davis, A.M., 1991. Fassaite composition trends during crystallization of Allende type B refractory inclusion melts. *Geochim. Cosmochim. Acta* **55**, 2635–2655.

Spivack, A.J., Beckett, J.R., Measures, C.I., Hutcheon, I.D., Wasserburg, G.J., 1987. The abundance and distribution of Be in Allende inclusions (abstract). *Lunar Planet. Sci.* **XVIII**, 938–939.

Sugiura, N., Shuzou, Y., Ulyanov, A.A., 2001. Beryllium–boron and aluminum–magnesium chronology of calcium–aluminum-rich inclusions in CV chondrites. *Meteorit. Planet. Sci.* **36**, 1397–1408.

Tomascak, P.B., Ter, F., Helz, R.T., Walker, R.J., 1999. The absence of Li isotope fractionation during basalt differentiation: measurements by multicollector sector ICPMS. *Geochim. Cosmochim. Acta* **63**, 907–910.

Wai, C.M., Wasson, J.T., 1977. Nebular condensation of moderately volatile elements and their abundance in ordinary chondrites. *Earth Planet. Sci. Lett.* **36**, 1–13.

Wark, D.A., Lovering, J.F., 1982. The nature and origin of of type B1 and B2 Ca–Al-rich inclusions in the Allende meteorite. *Geochim. Cosmochim. Acta* **46**, 2581–2594.

Zhai, M., Nakamura, E., Shaw, D.M., Nakano, T., 1996. Boron isotope ratios in meteorites and lunar rocks. *Geochim. Cosmochim. Acta* **60**, 4877–4881.